UNIVERSIDADE D
COIMBRA

José Pedro da Fonseca Sanches

DESENVOLVIMENTO DE REVESTIMENTOS DE WCTiN PRODUZIDOS POR PULVERIZAÇÃO CATÓDICA MAGNETRÃO COM IMPULSOS DE ALTA POTÊNCIA (HiPIMS) EM MODO DOMS

VOLUME 1

Dissertação no âmbito do Mestrado Integrado em Engenharia Mecânica no ramo/área de Produção e Projeto orientada pelo Doutor Fábio Emanuel de Sousa Ferreira e Doutor Ricardo Gil Henriques Serra apresentada ao departamento de Engenharia Mecânica, da Faculdade de Ciências e Tecnologia da Universidade de Coimbra.

Setembro de 2022

1 2  9 0

FACULDADE DE CIÊNCIAS E TECNOLOGIA
UNIVERSIDADE D COIMBRA

Development of WCTiN coatings produced by HiPIMS in DOMS mode

Submitted in partial fulfilment of the requirements for the degree of Master in Mechanical Engineering in the speciality of Manufacturing and Design

Desenvolvimento de revestimentos de WCTiN produzidos por pulverização catódica magnetrão com impulsos de alta potência (HiPIMS) em modo DOMS

Author

José Pedro da Fonseca Sanches

Advisors

Doutor Fábio Emanuel de Sousa Ferreira

Doutor Ricardo Gil Henriques Serra

Committee

Chair	**Professor Doutor João Carlos Barbas de Oliveira** **Professor Auxiliar da Universidade de Coimbra**
Member[s]	**Doutor Manuel António Peralta Evaristo** **Investigador da Universidade de Coimbra**
Advisor	**Doutor Ricardo Gil Henriques Serra** **Investigador da Universidade de Coimbra**

Coimbra, September, 2022

"You just keep pushing. You just keep pushing. I made every mistake that could be made. But I just kept pushing."

René Descartes

To my family and friends.

ACKNOWLEDGEMENTS

I'd like to express my gratitude to all the people who contributed directly or indirectly in making this work happen.

To Doctor Fábio Emanuel de Sousa Ferreira and Doctor Ricardo Gil Henriques Serra for being my mentors throughout this work. Their indispensable knowledge and availability to support me throughout this work was uncanny and I am truly appreciative for having the opportunity to learn from them.

I'd also like to extend all my thanks to colleagues belonging to CEMMPRE for their kindness and readiness to help whenever they could.

Last but definitively not least, to all my family and friends, without them I would not be the person I am today and their whole-hearted support undoubtedly made this work a reality.

Abstract

Hard coatings such as those of transition metal carbides/nitrides present great interest due to inherent properties of the elements that compose them. Taking tungsten carbide as an example, such properties englobe high melting point, extreme hardness, chemical inertness, oxidation resistance and good electrical conductivity, traits that are deep rooted in the advancement of material study and engineering for their desirability and usability in industrial applications such as fabrication of wear resistant coatings as well as cutting and drilling tools. Yet, such mechanical and tribological properties can be further improved with increasing amount of nanocrystalline ceramic phases. These coatings are prepared via various deposition processes. From various possible choices, magnetron sputtering seemed as the ideal candidate for deposition of a thin film that can attest to this objective, with attractive characteristics such as high attainable deposition rates, good adhesion, relative simplicity, and wide acceptance by the industry.

This work will consist of deposition and study of WCTiN thin film obtained by a co-sputtering method of deposition which is comprised of Direct Current Magnetron Sputtering (DCMS) and Deep Oscillations Magnetron Sputtering (DOMS), a variant of High Power Impulse Magnetron Sputtering (HiPIMS). For analysis and development of this hard coating, substrate polarisation and peak power of the HiPIMS source will be changed to understand its influence on the films mechanical and tribological properties, gathering information about the best performing coating.

Keywords: WCTiN, Co-Sputtering, HiPIMS, Tribology, Wear resistance.

Resumo

Revestimentos duros tais como carbonetos/nitretos de metais de transição apresentam grande interesse devido às propriedades inerentes dos elementos que os compõem. Por exemplo, carboneto de tungsténio possui propriedades como alto ponto de fusão, extrema dureza, resistência química, resistência à oxidação e boa condutividade elétrica, propriedades responsáveis pelo progresso no estudo de materiais e nas engenharias devido às suas aplicações industriais, nomeadamente criação de revestimentos resistentes ao desgaste e em ferramentas de corte e perfuração. No entanto, estas propriedades mecânicas e tribológicas podem ser melhoradas aumentando a quantidade de fase cerâmica nanocristalina. Estes revestimentos podem ser produzidos por diversos processos. A pulverização catódica assistida por magnetrão é um dos candidatos ideal para a deposição de revestimentos finos que conseguem atestar este objetivo, tendo características desejáveis como alta taxa de deposição, boa adesão, relativa simplicidade de processo e aceitação global na indústria.

Este trabalho consiste na deposição e estudo do filme fino de WCTiN obtido por um método de co-pulverização catódica com DCMS (Direct Current Magnetron Sputtering) e DOMS (Deep Oscillation Magnetron Sputtering), uma variante de HiPIMS (High-Power Impulse Magnetron Sputtering). Para análise e desenvolvimento deste revestimento duro será variado a polarização do substrato e a corrente de pico na fonte de HiPIMS, com o propósito de perceber a influência que estes parâmetros têm nas propriedades mecânicas e tribológicas de modo a desenvolver o revestimento com o melhor desempenho possível.

Palavras-chave: WCTiN, Co-Pulverização catódica, HiPIMS, Tribologia, Resistência ao desgaste.

Contents

LIST OF FIGURES

LIST OF TABLES

LIST OF SIMBOLS AND ACRONYMS/ ABBREVIATIONS

List of Symbols

Ar – Argon

C – Carbon

Cr – Chromium

Cu – Copper

DC_{int} – HiPIMS power source voltage charging value

N_2 – Nitrogen

O – Oxygen

S_q – Root mean square surface roughness

Ti – Titanium

V_{pin} – Worn volume in sphere used as pin

W – Tungsten

Acronyms/Abbreviations

AISI – American Iron and Steel Institute

AFM – Atomic Force Microscopy

BCC – Body-centred cubic

BIAS – Substrate polarisation

CoF – Coefficient of Friction

CVD – Chemical vapour deposition

DC – Direct current

DCMS Direct Current Magnetron Sputtering

DOMS – Deep Oscillation Magnetron Sputtering

EDS – Energy Dispersive Spectroscopy

FCC – Face-centred cubic

HEAs – High Entropy Alloy

HiPIMS – High-Power Impulse Magnetron Sputtering

HPPMS – High-Power Pulsed Magnetron Sputtering

MPPMS – Modulated Pulsed Power Magnetron Sputtering

PP – Peak Power

PVD – Physical Vapour Deposition

SEM – Scanning Electron Microscopy

XRD – X-Ray Diffraction

1. INTRODUCTION

Co-sputtered WCTiN is recently developed material with purposes of tribological applications in temperature demanding applications. Lack of knowledge on such thin film leads to a first assessment now developed in this work. The objective is to find and select the best parameters for its deposition concerning film composition, structure and microstructure, surface morphology and mechanical and tribological properties of the produced coatings. For a base analysis and comparisons, this material will be somewhat compared to transition metal carbides/ nitrides and HEAs, materials with relatable characteristics and chemical composition, to determine the best applicability of the WCTiN thin film.

Tungsten carbides (WC) present unique physical and chemical properties that has led to its continuous research and implementation [1]. The same is also true for titanium carbides and titanium carbon nitrides (TiC/TiCN) based materials [2,3], prominently with the purpose of developing films for application in cutting-tools [4]. High entropy alloys (HEAs) are currently entering the spotlight in material development with attractive and comparable properties such as high hardness, great wear resistance, good fatigue resistance, excellent high temperature strength, thermal stability and good oxidation and corrosion resistance [5,6], properties that are inherent on all mentioned types of materials.

Fabrication of WCTiN is obtained by co-sputtering of DCMS (direct current magnetron sputtering) and HiPIMS (High-Power Impulse Magnetron Sputtering) on different targets, a method that was proven a successful endeavour [7,8] with a proven record to be a reliable source for development of coatings with a wide range of properties [9].

For context in the early assessment of this newly fabricated hard thin film, some comparable materials include nanocomposites thin films such as TiN, with typical CoF of 0.7 while WC nanocomposites systems can range as low as 0.03 in vacuum and 0.15 in air [10,11], so it will be interesting to see where WCTiN will land. TiC and Ti(CN) based cermets are also known coatings for use in aggressive environments, proven has highly resistant to corrosion and usable at high temperatures, yet sensible to the type of wear mechanism it endures [2,12]. WCTiN thin films were produced with a TiN interlayer and tribological studies on TiN/TiCN/DLC composites clearly indicate an increase the total

hardness of the coatings [13]. Scratch testing done in TiN thin films shows that typical behaviour will be the formation and propagation of perpendicular cracks to the moving indenting stylus with increasing microcracks. Then at high loads detachment of film particles [14]. Meanwhile WC and related hard metals scratch test determined that wear damage is mostly WC grain fracture on indented area with plastic slip on the edges of the scratch [15,16].

In this study it is evaluated the tribological and mechanical properties of WCTiN, a new transitional carbonitride thin film that has the potential to inherit the desirable properties present in WC/TiC/TiCN and HEA type materials, and study how its properties are influenced by the substrate polarisation and the HiPIMS peak power. Chemical, structural, morphological, mechanical and tribological characterization was performed to verify the films characteristics and rank their tribological performance.

2. STATE OF THE ART

2.1. Magnetron Sputtering

During the XVIII century, some researchers discovered that when discharged an electric current between two electrodes under a thin atmosphere, some of the cathode material would deposit on the anode and all over the chamber walls, a process later denominated as sputtering. Sputtering is a type of physical vapour deposition (PVD), technology that can be summarized in three phases: firstly, transforming the material to be deposited into a gas; secondly, the transport of this gas from source to substrate; lastly, condensation of said material onto the substrate in order to form coatings that could reach thickness as thin as the atomic scale [17]. PVD, technology widely used for deposition of thin films with varying characteristics and many demands, from aesthetics to tribological performance, was a term first coined in the 1960's. In the last decades, evolution of PVD techniques resulted in its use on thin film production with the objective of improving the deposition rate and coating properties, suited to diverse technological needs. In recent years, it has become more prevalent on coating tools [18].

Magnetron sputtering is a technique that has rapidly gathered interest and popularity in recent decades, mostly due to the ever-increasing need for high quality functioning coatings in a multitude of markets. With the introduction of the "balanced" magnetrons in the early 1970's and its development up to recent years, this technique has been responsible for many advancements in thin film fabrication. In the basic sputtering process, a cathode (target) plate is bombarded with energetic ions (plasma) causing the ejection of atoms from the target, some of which will then condensate on the substrate and consequently grow the film. A secondary emission of electrons occurs from the target surface, a consequence of the ion bombardment, that plays an important role in keeping the discharge plasma that feed the ejection process from the target. Many materials were deposit using this basic method, however, the process is not without its flaws, such as low deposition rates and high substrate temperatures. Magnetron sputtering, as its name would suggest, makes use of a magnetic field that can sustain the secondary electrons motion around the targets. This essentially results in higher probability of electron-atom collision and because of this, the process allows

for higher deposition rates with more efficient ionization, permitting sustained sputtering at lower operating pressures with lower voltages [9,19].

The simplest form of use of magnetrons is deposition of metallic materials with DC (direct current) source. DCMS is the cheapest of the magnetron processes due to the simplicity of manufacturing DC power supplies. Yet sputter sources, despite providing good coverage for deposition on the substrate, it is not perfect, as directional deposition of material and statistical nature of the process, it is common to create some more dense areas than others, which will feed furthermore the geometrical unbalance of the film, like "rain on mountains", some spots will be more difficult to reach as result of directional deposition, reiterating the unbalanced density of the coating. A way to combat this effect and improve deposition quality is with the application of voltage on the substrate, leading to surface bombardment of the growing film with positive ions, similar to the process occurring in the targets during the sputtering. This causes an increase in ions energy and some re-sputtering of the coating layer, effects that allow higher control of film growth process and decreased defects such as microcracks [20,21].

DC reactive magnetron sputtering was the next prominent advancement, this method consists in sputtering of elemental targets in the presence of a chemically reactive gases that mass react with both ejected target material and surface target material. Very popular nowadays for deposition of a wide range of thin films that are composed with oxides, nitrides, carbides, fluorides or arsenides. Advantages in this process are such as deposition of thinner films and controlled stoichiometry and composition at high deposition rates and on industrial scale, and ease of fabrication of high purity elemental cathodes. Nevertheless, reactive sputtering does have its hurdles as does everything, for it is a complex non-linear process with several parameters. Target poisoning is constant concern in DC reactive magnetron sputtering, which can be mostly attributed to the formation of a compound layer on the target surface which has a different secondary electron emission, and a so-called gettering process, which describes the chemisorption of the reactive gas on the target material deposited on the substrate [22-24].

2.2. High-Power Impulse Magnetron Sputtering

In DCMS the plasma density can be increased by increasing the power to the target. Yet this is a limited application as the cathodes are limited by their melting point and cooling efficiency of the target. In HiPIMS, also known as HPPMS (High-Power Pulsed Magnetron Sputtering), the power is applied in very short pulses, meaning instantaneous power to cathodes can be significantly amplified while still averaging the same power as DCMS sources, a technique was introduced by Kouznetsov in 1999. As the nature of the process is time dependent and composed of pulses, the drawback of HiPIMS compared to DCMS is lower deposition rates, ranging from 30 % to 80 % of its rate [25].

Since long it has been a goal to combine magnetron sputtering with ion assistance for film growth, and as a result technologies such as HiPIMS were developed to supply ions that can assist in film formation more efficiently, since these ions become part of the growing film. Coatings synthesis with the plasma phase is often called energetic deposition (or energetic condensation) due the kinetic and potential energy that plasma ions bring to the film growth process. The range of kinetic energies from the particles can reach hundreds of electron-volts, exceedingly often the displacement energy of atoms near the surface. Since HiPIMS requires high currents is therefore used with conductive metal targets. All metal atoms have significantly lower first ionization energy than noble gases, so they are readily ionized in the magnetron plasma provided they do not travel too fast from the target surface through discharged plasma. Once ionized, the newly formed metal ion is accelerated by the local electric field which routes it into the target, so called self-sputtering. Sustained self-sputtering without process gas is unattainable since most target aterials do not have high self-sputtering yield. Typically, it is used argon for being an inert and inexpensive gas, and it's believed that repeated supply of gas neutrals contributes to high current levels. Gas ions, such as argon atoms are not bonded in the film growth, returning to pre target region, where the ionization and neutralization cycle repeats [26].

Modulated Pulsed Power Magnetron Sputtering (MPPMS) is a variant of HiPIMS capable of producing high ionization fraction of sputter target species and at the same time achieving higher deposition rates. Recent studies on the properties of plasma utilized in HiPMS for different target materials, reached the conclusion that the degree of ionization of the targets is strongly affected by peak pulse power and its material, with some reports even claiming that the fraction of ionized sputtered material can be increased up to 70% or higher

for Cu and Ti [27]. This technology allowed for greater control in flux of sputtered species, consequentially in controlling of the kinetic effects in film growth. Due to nature of HiPIMS and MPPMS technology, much higher target voltages and currents are used and the lack of positive reversal voltage between impulses facilitates arc generation, which in turn demands sophisticated hardware for its handling. DOMS (Deep Oscillation Magnetron Sputtering) is a new proposed design of MPPMS, with aim to reduce arc generation. This goal is achieved by use of voltage oscillation packages with short off-time periods, instead of using short "digital conversion from analogue waves" type of voltage pulses to modulate peak power, which has been shown to allow virtually arc-free deposition for reactive deposition of insulating films [28].

2.3. WC, TiC and TiCN based materials

Transition metal carbides such as WC and TiC are refractory compounds that possess high hardness and strength at high temperatures. The main disadvantages of ceramics is their covalent bonding nature, making them brittle and difficult do densify. To address shortcomings such as these ones cermets were developed, a class of composite structural materials that utilizes metallic binders to obtain dense bulk materials based on refractory ceramics such as aforementioned WC and TiC. These materials have been used extensively in various engineering applications, such as cutting tools, rock drill tips, general tools and general wear coatings too, and more recently advocated to be used in catalytic converters as well as microelectronics. It is common knowledge now that the softer metallic phase from crystalline sintering processes of WC based transition metal carbides (powder metallurgy) limits the performance and hinders its use in higher temperatures, so most recent attempts of development focus on attempting to obtain near theoretical density by replacing fully or partially the metallic binder phase with ceramic sinter-additives [29,30].

TiC and TiCN based cermets have seen a surge in recent years also regarding the cutting tool industry. When the two are compared, TiCN have much higher hardness at high temperatures, higher transverse rupture toughness and better resistance to oxidation. TiCN cermets were first created in 1930's but was only in the 1970's that its interest rise. The more developed industrial nations took account for most of the production and in the 1990's, TiCN-based cermet cutting tools had about 30% of market share in Japan. Nowadays this

material is used mostly in cutting tools. These tools are used at high speed finishing and semi-finishing of carbon steels and stainless steels. Due to the excellent properties at high temperature and low density, this material is also used in more high performing applications, such as refractory parts in jet engines, turbine engines and both gasoline and diesel engines; in the field of oil and mining they are used not only on drills and excavating tools, but as well in oil nozles and throttles. The appeal of TiCN based cermet is the combination of properties from TiC and TiN, such as high hardness, high melting point, good corrosion resistance, excellent wear resistance, good chemical stability, high thermal and electric conductivity. The disadvantage it's how brittle the material is and as such typically used as the hard phase on composites [2].

2.4. High Entropy Alloys

High entropy alloys are multicomponent mixtures of at least five elements in similar concentrations, where the high entropy from the mixing can stabilize disordered solid solution phases with simple structures like body-centred cubic (BCC) or face-centred cubic (FCC) in competition with ordered crystalline intermetallic phases that often contain complex giant unit cells. In order to obtain high entropy of mixing, the alloys must be composed from 5 to 13 major elements in similar concentrations, ranging from 5 to 35 At. %, so obviously the number of possible HEAs is practically unlimited.

The need of better and newer materials is both a consequence and need for modern technology, as improvements are made in all industries. This necessity is particularly high in industries such as aerospace, power production and high-speed manufacturing machinery, whereas properties such as strength at high temperature and lightweight is key for structural efficiency. HEAs are recently being studied and are still new in material science and engineering. One of the most attractive characteristics is that the specific mechanical properties of an HEAs can be tailored made based on its chemical composition and crystalline structure (the most significant aspect of its microstructure). Demand for this type of material is currently very high as, unlike conventional alloys, HEAs have better hardness at high temperatures. This is due to multiple hardening mechanisms such as dislocation reactions, secondary phase strengthening and single solid phase strengthening.

In HEAs, mechanical properties can vary from its constituent elements, as structure types are the dominant factor for controlling the strength or hardness in these materials. BCC

structured HEAs usually have very high yield strength and limited plasticity while FCC structured ones have low yield strength and high plasticity. So, a mixture of BCC and FCC is expected to have balanced properties, both high strength and good ductility. As studies show, the main disadvantage is in some microstructures of certain HEAs, is that they can be very complicated, often undergo in spinodal decomposition, a mechanism where a single thermodynamic phase spontaneously separates in two phases without nucleation. This leads to disordered phases precipitation at lower temperatures. And since HEAs usually withstand high temperatures, solution strengthening mechanisms will be hard to achieve [31-34].

2.5. Tribology

Tribology was first defined in 1967 by a committee of the Organization for Economic Cooperation and Development, a new field in science which focuses on friction, wear and lubrification of interacting surfaces in relative motion. Wear is the main cause of material wastage and loss of mechanical performance. Reduce and control the effects of wear is always a concern in engineering. The main problem in wear is friction, so controlling it can lead to significant savings in material and energy. The energy losses are significant and estimated as one-third of the world's energy resources to overcome the challenge [35].

Surface coatings and surface modifications aim to enhance tribological performance and other physical and chemical properties of solid surfaces. Regarding hard coatings, nitrides, oxides, carbides and borides have been extensively used, formed either by chemical vapour deposition (CVD) or previously discussed PVD. Investigated crystal orientation effect of CVD on Ti(C,N) found that the preferential orientated coatings exhibited a 20 % higher wear resistance and 35 % better abrasion resistance compared to reference coating. Coatings such as TiAlN, TiCN and AlCrN deposited either by PVD or CVD processes are widely used as wear resistant at high temperatures [36].

Surface roughness defines the random deviations of peaks and valleys that make the three-dimensional topography of any surface. In manufacturing engineering, controlling the texture of the surface of machine parts is needed, defining the quality of design at any stage of manufacturing. Mathematical representation of surface feature can be done in several ways. Analogue solutions consider a fictitious line for obtaining the mean height line, which is basically the average height of a surface. From this we can determine what is called root

mean square roughness (S_q), an expression used to measure the standard deviation of the distribution with respect to the mean line [37].

Coefficient of friction (CoF) has long been used for scientific purposes, it is easy to define as a ratio of two forces acting, respectively, perpendicularly and parallel to an interface between two bodies under relative motion or impeding motion. The energy that is transformed because of frictional contact can be stored in the system, associated with microstructural defects, or dispersed in several ways such as heat, vibration, material deformation or the creation of a new surface. Therefore two materials with the same CoF can have completely different behaviours. The interrelationship between friction and wear also changes with time. Usual exists a running-in period when registering CoF between two solid materials, as a result of the energy stored or dispersed for initial time of the test [38].

3. EXPERIMENTAL PROCEDURE

Since the purpose of the dissertation was both tribological and mechanical evaluation of the newly produced WCTiN thin films, there was a strong practical component to this work. This involves testing and measuring the films properties and how changing parameters affects this developing coating on several properties such as its hardness, surface morphology, composition, specific wear rate, coefficient of friction and film adhesion. In order to try pinpoint best deposition parameters for WCTiN thin film, two series were produced, one designated as "BIAS series", where different substrate polarisation were attempted for a constant peak power of 59 kW, and another series attributed as "PP series", where varying values of peak power were tried on the Ti target for a constant substrate polarisation of -40 V.

3.1. Deposition of WCTiN

WCTiN coatings were fabricated using a combined sputtering method composed of DCMS for a tungsten carbide (WC) target with an ENI RPG50 power source, and DOMS for a titanium (Ti) target, powered by a Cypirum™ plasma generator from Zpulser Inc. Reactive atmosphere was used during the deposition composed of argon (Ar) and nitrogen (N_2). In DOMS a pulse is generated during1800 μs which is sub-divided in 25 oscillations each with 6 μs on-time and 64 μs off-time, giving rise to 1.8% duty cycle, as shown in Figure 3.1.

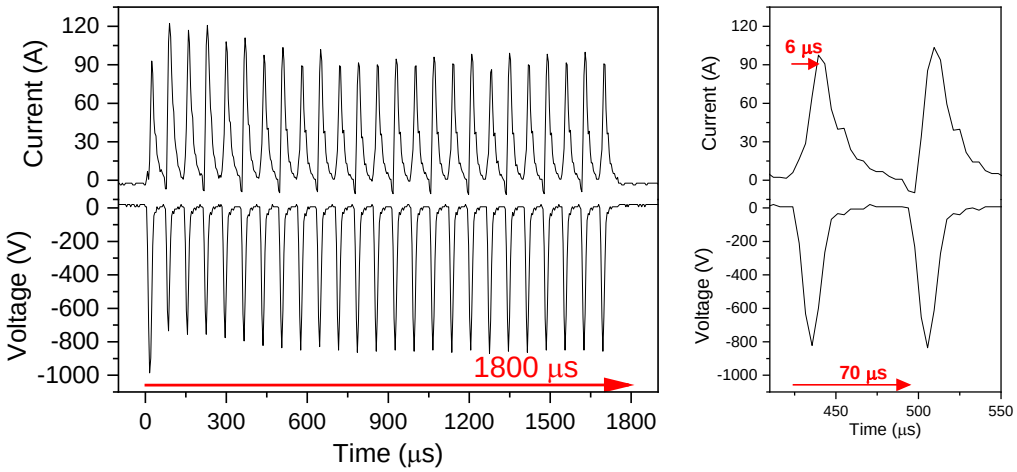

Figure 3.1. DOMS pulse utilized for WCTiN deposition.

For a more comprehensible approach in studying this thin film, two series were prepared: one was the substrate polarisation that is increased negatively for 0, -40, -60, -80 V, and a second focused on peak power influence on the thin film with the samples, using 44, 59, 89 and 105 kW peak power. More detailed deposition parameters are shown in Table 3.1.

			DCMS		DOMS			
Series	**DC_{int}**	**bias**	**Voltage**	**Current**	**Frequency**	**Voltage**	**Current**	**Power**
	(V)	(V)	(V)	(A)	(Hz)	(V)	(A)	(kW)
BIAS	350	0	435	1.6	100	1112	55	61
BIAS/PP	350	-40	444	1.6	100	1100	54	59
BIAS	350	-60	458	1.5	93	1167	55	64
BIAS	350	-80	450	1.6	87	1150	55	63
PP	330	-40	440	1.7	119	1020	43	44
PP	370	-40	436	1.6	79	1215	73	89
PP	390	-40	437	1.6	73	1260	83	105

Table 3.1 Deposition parameters for WCTiN films prepared. DCMS applied to WC target and DOMS to Ti target. Values for DOMS represent their peak value.

All samples were deposited on silicon and M2 steel substrates, geometrically measuring 25 mm in diameter and, during deposition, distanced with 80 mm from both targets, rotating at 23.5 rpm with 150x150x8 mm equally dimensioned targets (WC and Ti).

In preparation for all samples, ultrasonic cleaning was performed (10 + 10 minutes in acetone followed by ethanol, respectively). Lower than 1.8x10-4 Pa base vacuum is obtained in the chamber before an etching step on the substrates is performed using a pulse power unit running at 350 V, 120 kHz and 1616 ns pulse on-time in Ar atmosphere at 0.4 Pa for 60 minutes. This is then proceeded by creating an interlayer with the following steps:

1 – Chamber at 0.4 Pa; HiPIMS at 700 W; DCint = 300 V; Ar = 8 sccm (0.4 Pa).

2 – Ti interlayer for 10 min.

3 – Gradually increase N2 to 24% for 1 minute.

4 – Gradually increase N2 to 48% for 1 minute.

5 – Gradually increase N2 to 72% for 1 minute, adjust gate for 0.8 Pa.

6 – Gradually increase N2 to 100% for 1 minute, adjust gate for 0.8 Pa.

7 – Increase DCint to 330 V.

8 – TiN interlayer for 6 minutes.

9 – Switch on WC at 300 W for 1 minute before previous step ends.

10 – Adjust pressure with gate to 0.8 Pa.

11 – Increase WC power to 700 W in steps of 100 W for 30 seconds each.

12 – Adjust pressure with gate to 0.8 Pa.

13 – Increase DCint to 350 V.

14 – Adjust HiPIMS DCint and bias (from 40 V) to the final deposition value.

After these steps, the deposition is done for 50 minutes at 0.8 Pa (0.4 Pa Ar + 0.4 Pa N2) with varying parameters (Table 3.1) to obtain the different samples and proceed with its study.

3.2. Scanning electron microscopy

Scanning electron microscopy (SEM) was used to obtain the WCTiN film thickness, cross-section structure and surface morphology with Zeiss Merlin Gemini II equipment, using 2 keV electron beam for cross-section and surface area. Surface SEM analysis after pin-on-disk testing was performed in another equipment, Hitachi model SU3800, using 10 kV acceleration.

3.3. Energy Dispersive spectroscopy

Composition of WCTiN films was obtained via energy dispersive spectroscopy (EDS) system integrated with the SEM equipment. As-deposited WCTiN films composition was obtained with EDS in Zeiss Merlin Gemini II equipment, The SEM Hitachi model SU3800 coupled with a Bruker Quantax Compact EDS detector was utilized for composition analysis of the film, pin and resulting debris after tribology characterization.

3.4. Atomic force microscopy

Surface morphology of the thin film was registered by atomic force microscopy (AFM), operated on a Bruker Innova system fitted with a silicon tip with less than 8 nm tip radius, working in tapping mode for scans with 3x3 micrometre. Plane and polynomial background levelling was performed in all images to obtain only the samples surface roughness excluding external influence (tilting and bow) using Gwyddion software.

3.5. X-Ray diffraction

Measurements for XRD (X-Ray diffraction) were taken out of a PANalytical X´Pert PRO MPD with Cu Ka radiation at 45 kV and 40 mA. This system operates with parallel beams in q – 2q geometry, incident beam optics made with a hybrid monochromator with Cu W/Si mirrors and double crystal Ge (220). A parallel plate collimator (0.7º) and a Soller slit (0.0004º) is mounted on the path of the diffracted beam, with a PIXcel detector in receiving slit mode used for X-ray collection.

3.6. Hardness and reduced Young's modulus

To measure both hardness and reduced Young's modulus it was used a Micro Materials Nano Tester as nano-indentation type equipment, this one equipped with a Berkovich pyramidal diamond indenter. The hardness was evaluated from load-displacement curves using depth-sensing method, executing 16 measurements for each sample with a load of 5 mN, ensuring that the indentation depth never reach 10% of the total film thickness. Table 3.2 and Table 3.3 sow the maximum penetration depths achieved during the hardness measurements for the two studied series.

Substrate polarisation (V)	**0**	**-40**	**-60**	**-80**
Max. depth (nm)	121	108	91	120

Table 3.2 Maximum depth achieved with nano-indentation with 5mN load for the samples prepared with different substrate polarisation.

Peak power (kW)	**44**	**59**	**89**	**105**
Max. depth (nm)	108	108	119	106

Table 3.3 Maximum depth achieved with nano-indentation with 5mN load for the samples prepared with different peak power.

3.7. Scratch test

Utilizing an automatic scratch tester, a CSEM – REVETEST fitted with a Rockwell "C" diamond-tipped indenter with a spherical tip radius of 100 μm, scratch test analysis of the adhesion of WCTiN on the substrate was made. The parameters for this evaluation consisted of a normal load increasing linearly 100 N/min, up to to 60 N in testing, with 10 mm/min speed. Specimens and indenter were cleaned with ethanol, and after the test itself the samples properties were quantified using an optical microscope, a Leica DM4000 M

LED, equipped with a Leica MC120 HD amplification and observed at maximum magnification with a HCX PL FLUOTAR L 20x/0.40 BD lens.

3.8. Coefficient of friction

Results for coefficient of friction (CoF) originated from a homemade pin-on-disk equipment. For these tests it was used a 10 mm steel ball (AISI 52100) as pin with 5 N load for 4000 cycles at 0,1 m/s. Two radius and respective rotating speed were used, 159.2 rpm for a track of 6 mm diameter, and 119.4 rpm for 8 mm diameter track.

3.9. Specific wear rate

The tracks obtained in the pin-on-disk test were analysed with a 2D profilometer (Mitutoyo Surf test SJ-500) to calculate the wear, measuring on 3 equally distant profile points of the tracks to achieve specific wear rate for the WCTiN coating, calculating the volume of the track depth and using then equation (3.1). Specific wear rate was also obtained for the spheres (pin) using images obtained from SEM device and then measuring two perpendicular diameters to quantify the wear volume lost for the pin using equation (3.2).

The equations used were the following:

$$Specific\ wear\ rate\ (track) = \frac{Area\ *\ Perimeter}{Force\ *\ Distance}\ [m^3/\ N.m] \tag{3.1}$$

$$Specific\ wear\ rate\ (pin) = \frac{V_{pin}}{Force * Distance} \tag{3.2}$$

For equation (3.1), $Perimeter$, $Force$ and $Distance$ are constant throughout calculations, with $Force$ always equal to 5 N as used in experimentation and the others as stated:

$$Perimeter = \pi * 2 * 0.008\ [m] \tag{3.3}$$

Resulted from standard perimeter equation for a track radius of 8 mm and then inserted in distance for 4000 cycles:

$$Distance = Perimeter * 4000\ [m] \tag{3.4}$$

The difference between volume on (3.1) and V_{pin} is that the first is a computer calculated from single points, iterated for $Area$ values measured on points with the profilometer, therefore in need of its multiplier ($Perimeter$) for achieving track volume, while in V_{pin} the performed distance is already accounted, seen on equation (3.5).

$$V_{pin} = \frac{\pi * {d_p}^4}{64 * 5} \ [m^3] \tag{3.5}$$

From equation (3.5) d_p refers to median distance of cross section from contact area on the sphere used in pin-on-disk, 5 as in the 5 mm radius of the pin (10 mm steel ball AISI 52100).

4. RESULTS

For a clearer understanding of WCTiN thin film properties and how its deposition parameters influence their properties, the results will be organized separately for the two produced series. On an additional note, one sample is shared within the two series; the one with -40 V of substrate biasing is the same as the one identified with a 59 kW of peak power, typically identified in the figures as "b)" with the exemption of Figure 4.16.

4.1. BIAS series

4.1.1. Composition

In Figure 4.1 there is a representation of the WCTiN composition obtained by EDS.

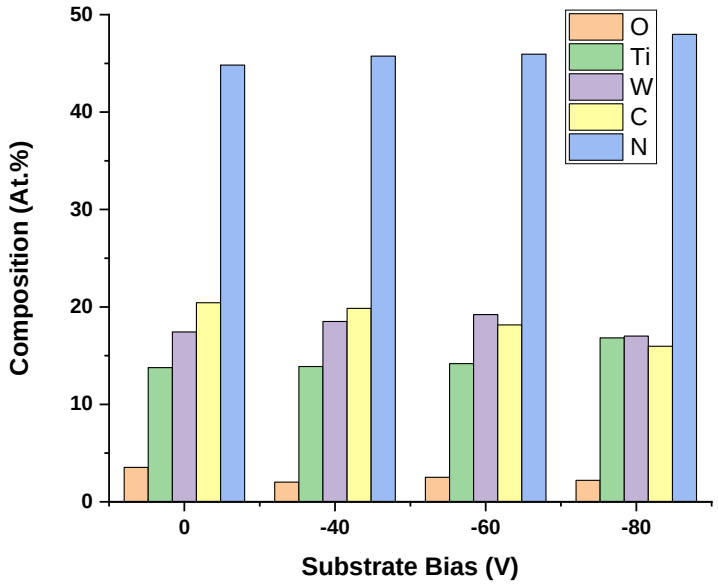

Figure 4.1. Composition of WCTiN films with different substrate polarisation obtained through EDS.

It can be noted that with the negative increase of substrate polarisation the atomic percentages of nitrogen and titanium experience a steady increase as well, N increasing from 44.8 at. % to 47.9 at. % while Ti goes from 13.8 at. % to 16.8 at. %. With increasing bias, there is also a decrease in the concentration of carbon, from 20.4 at. % to 15.9 at. %. Substrate polarisation seems to have no discernible impact on tungsten concentration, averaging 18 at. %. Traces of oxygen are always present as a result of surface contamination of the specimens when exposed to the atmosphere, rounding to 2 at. % in the thin films.

4.1.2. Structure

XRD spectra of WCTiN films can be observed in Figure 4.2. All samples show similar results for this series.

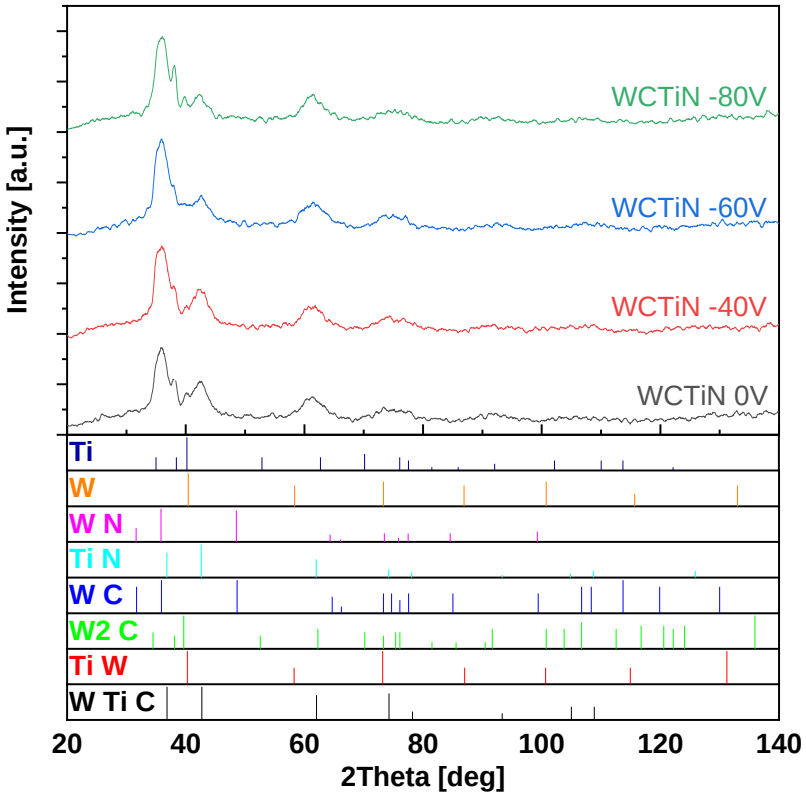

Figure 4.2. XRD spectra for WCTiN films with varying substrate polarisation. The reference pattern for Ti, W, WN, TiN, WC, W2C, TiW and WTiC are also displayed in the spectra.

It can be said with confidence that substrate polarisation does not play a substantial role in film growth, and thus the same is also true for film structure. Shifted, the low intensity peaks of WTiC appear for all the samples, assuring then a clear influence of N on WCTiN formation. Although traces of WC peaks are found throughout the different specimens, no complete indexation is obtained, confirming decarburization of WC during the sputtering process. TiN, TiW and WN display partially indexed peaks which further corroborates WC decarburization.

4.1.3. Microstructure

Figure 4.3 details us a closer look at the films' microstructure from cross-section perspective SEM micrographs.

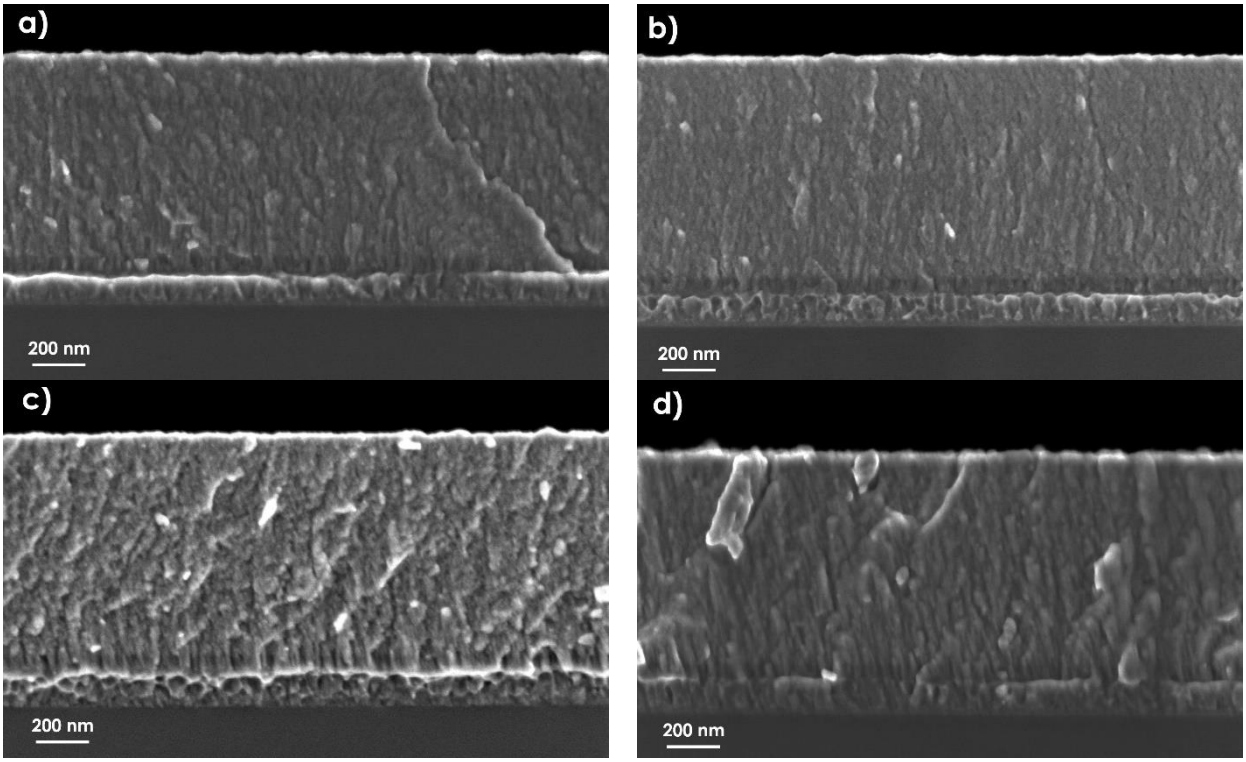

Figure 4.3. SEM cross-section micrographs of WCTiN films prepared with substrate polarisation of: a) 0 V; b) -40 V; c) -60 V; d) -80 V.

As seen in Figure 4.3, the film does not appear to be influenced by negatively increasing the substrate bias voltage. The micrographs show the 100 nm Ti interlayer followed by the WCTiN film without significant differences between them. The micrographs show a dense cross-section with only the initial part of the film (next to the interlayer) with a clear columnar microstructure. This being said, all the thin films present dense microstructure.

4.1.4. Surface morphology

In Figure 4.4, the SEM surface micrographs of the WCTiN films complement the information shown in Figure 4.3. All the samples show cauliflower-like surface morphology, confirming that the substrate polarisation has no effect on the WCTiN coatings. The surface features size and distribution are similar in all four samples.

AFM of the WCTiN films are very similar (not shown), indicating that the substrate polarisation does not play a particular role in defining the surface morphology, confirming the SEM surface micrographs results of Figure 4.4. The roughness parameters collected and presented in Table 4.1 confirm the similar surface, with a positive skew value in all samples, meaning that the surface has more positive features than negative.

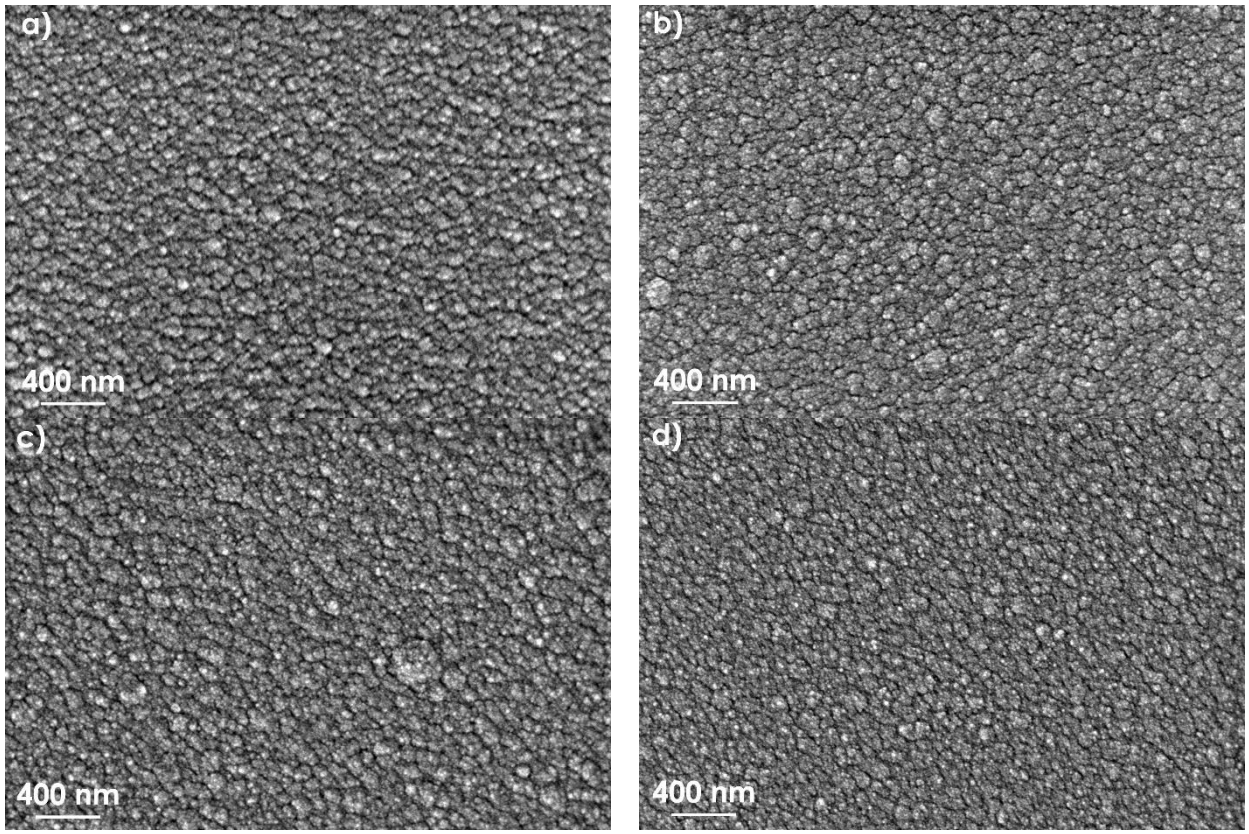

Figure 4.4. SEM micrographs of WCTiN films surface with substrate polarisation of: a) 0 V; b) -40 V; c) -60 V; d) -80 V.

Bias (v)	**0**	**-40**	**-60**	**-80**
S_q (nm)	4.98	5.73	4.52	5.14
Skew	0.28	0.49	0.45	0.26

Table 4.1 Surface roughness values for bias WCTiN samples obtained using AFM.

4.1.5. Mechanical properties

Hardness and reduced Young's modulus measurements for this series is displayed on Figure 4.5, obtained with load of 5mN.

It is clearly an increased tendency from 15 until 29 GPa as negative bias is increased up to -60 V. Further negative substrate bias, -80V, shows a dramatic decrease of the hardness back to 16 GPa. Reduced Young's modulus also accompanies hardness in tendency, increasing and decreasing as such. From this data, the best performing thin film is the -60 V sample, with the biggest increment with substrate polarisation influence, rising by 10 GPa from -40 V.

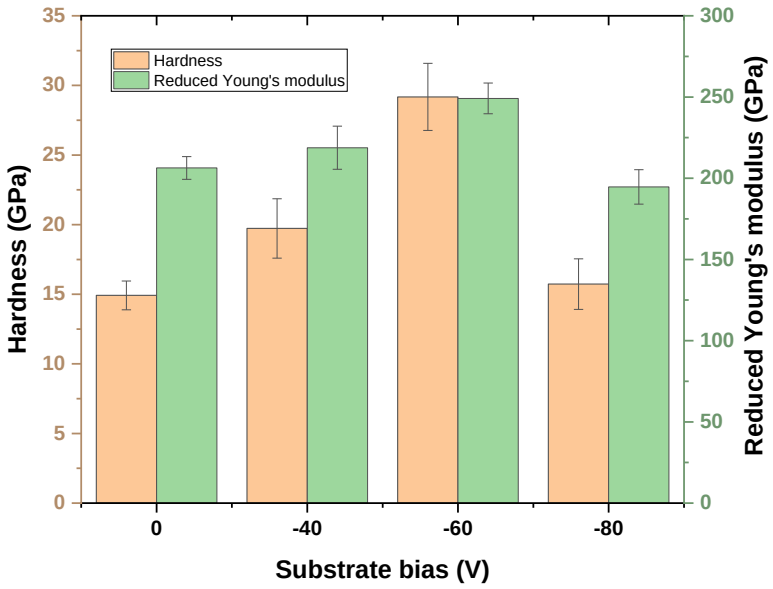

Figure 4.5. Hardness and reduced Young's modulus were obtained with a 5 mN load for different substrate biasing.

Further data on maximum depth measurements taken in testing performed to WCTiN coating is registered in Table 3.2, confirming that during the hardness measurements, we can exclude substrate influence from hardness.

Optical images of the performed scratch tests on WCTiN films prepared for this work can be seen in Figure 4.6.

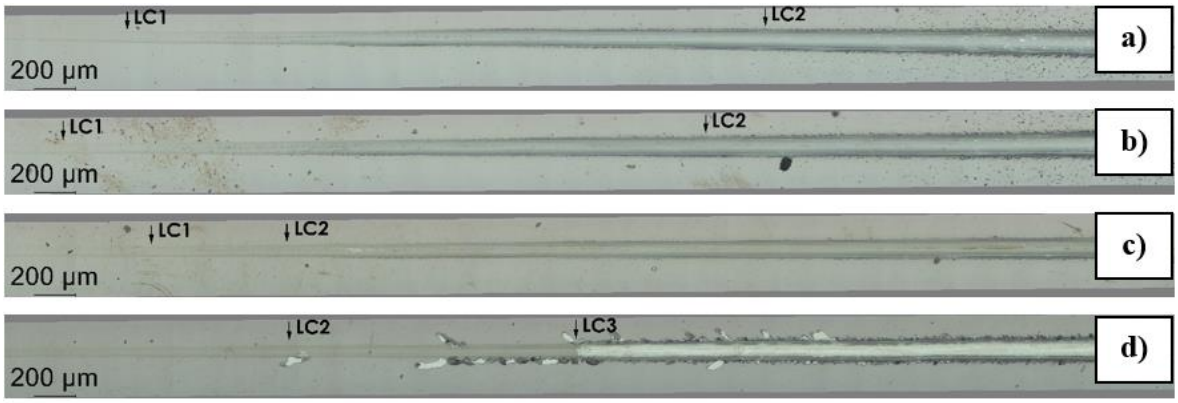

Figure 4.6. Scratch images obtained with an optical microscope after scratch test on samples varying substrate biasing: a) 0 V; b) -40 V; c) -60 V; d) -80 V.

Starting with the 0 V substrate polarisation sample, an LC1 type failure occurs after 6.6 N, extending and becoming more prominent at 11.8 N with clear vertical cracks increasingly accentuated and reaching the sidewalls. At 37.4 N, an LC2 type initiates with

delaminated points on the film. The -40 V sample behaves similarly to the 0 V one, with an LC1 failure beginning at 3.4 N with likewise propagation, followed by LC2 failure at 34.8 N. Regarding the -60 V coating, the LC1 failure is observed at 9.4 N and LC2 at 17.2 N. However, unlike previous samples and despite the LC2 failure earlier comparatively, the surface is less damaged with seemingly random LC2 type failures that do not increase proportionally in number with the increasing force as the test proceeds. In fact, until the end of the test, the film maintains its appearance without an increase of failure. The -80 V coating starts off with a very visible LC2 failure at 14.2 N, later developing and turning into an LC3 type failure at 28.8 N with complete failure and delamination of the coating. This behaviour, in conjunction with the drop of hardness seen in Figure 4.5 indicates a clear compromise due to internal stress forces, which have been documented on similar materials [39].

4.1.6. Tribological properties

The Coefficient of friction results obtained for the WCTiN films prepared with varying substrate polarisation are displayed in Figure 4.7.

The results show a coherent behaviour, and all the samples have similar CoF values in the steady state period of the curve, around 1.14. The running-in period is sharp and short in all samples between 100 and 150 cycles, exempt for -60 V. This film shows a slower and less sharp running-in period during 250 cycles. Another difference was the WCTiN with 0 V substrate polarisation higher CoF of 1.41 at the beginning of the test but after the running-in period. The CoF then stabilizes in the same value as for the other samples, around 1.14.

One interesting point is the CoF signal instability during the testing. The first group composed of 0V and -40 V, had more unstable CoF behaviour throughout the test. The second group composed of -60 V and -80 V, demonstrated a smother CoF curve along all the tests.

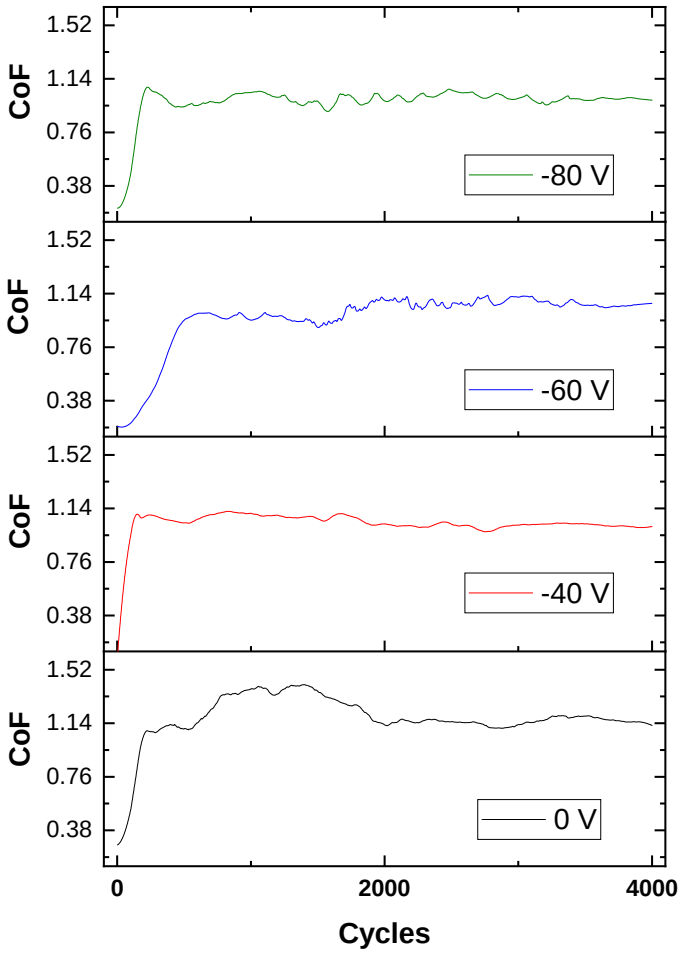

Figure 4.7. CoF results of WCTiN films prepared with different substrate polarisation; pin-on-disk test ran for approximately 200 m with a load of 5 N.

The SEM micrographs of the contact point in the pin used for the pin-on-disk tests are presented in Figure 4.8.

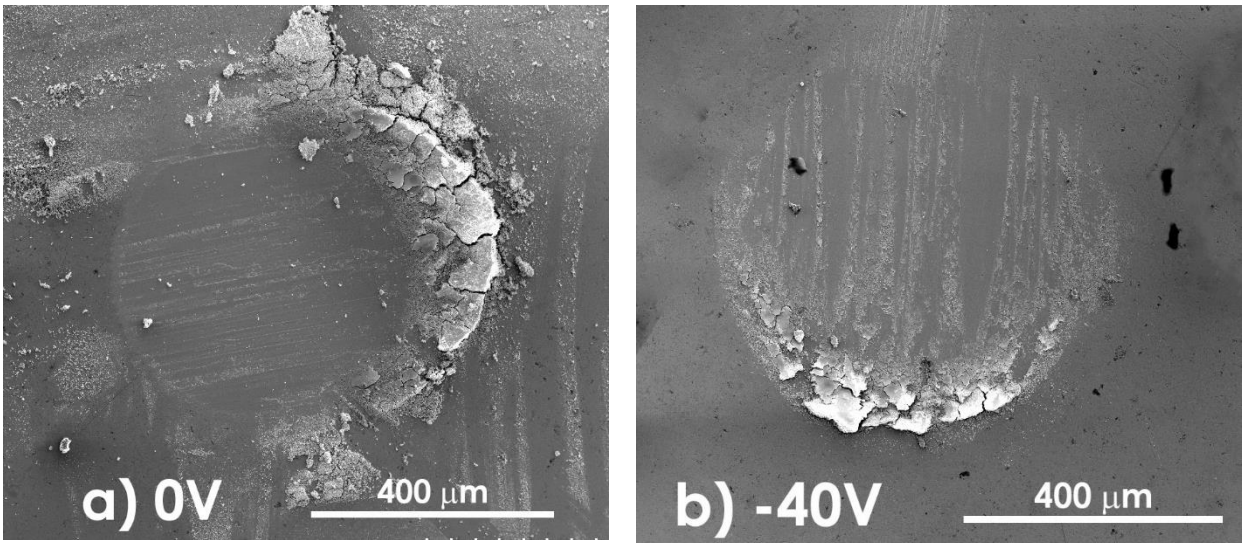

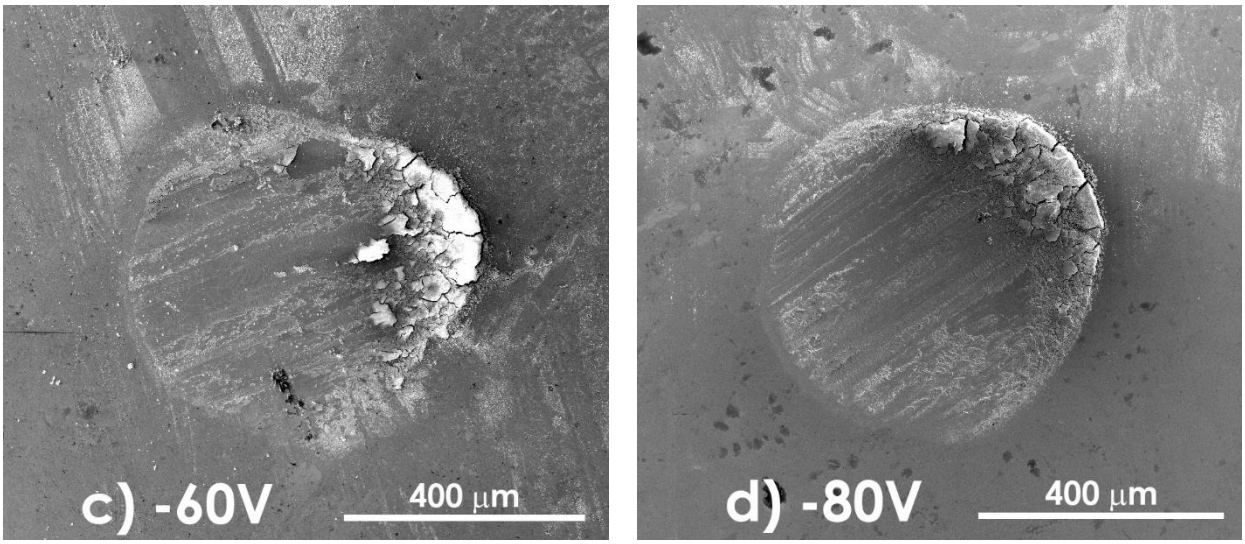

Figure 4.8. SEM micrographs of the pin contact point used in the tribology testing for substrate polarisation of: a) 0 V; b) -40 V; c) -60 V; d) -80 V.

All micrographs of the contact point for the coatings have an accumulation of wear debris around the edges of the worn area. There are also signs of wear inclusions of coating particles in the worn area. The main difference between the contact area differs between 0 V and -40 V samples compared with -60 V and -80 V, being the latter two the ones with a smaller worn area. Further examination was conducted on the composition of the debris on both film and pin, confirming that material transfer had occurred mutually.

The SEM micrographs of the wear tracks for the WCTiN films after pin-on-disk testing are shown in Figure 4.9.

The most obvious observation is the amount of transferred material going into the wear track proportionally increases with the increase of negative substrate polarisation. The quantity of side material is similar in all samples. Since all tracks are equally scaled, it can be said that the wear track width was not influenced by the substrate polarisation.

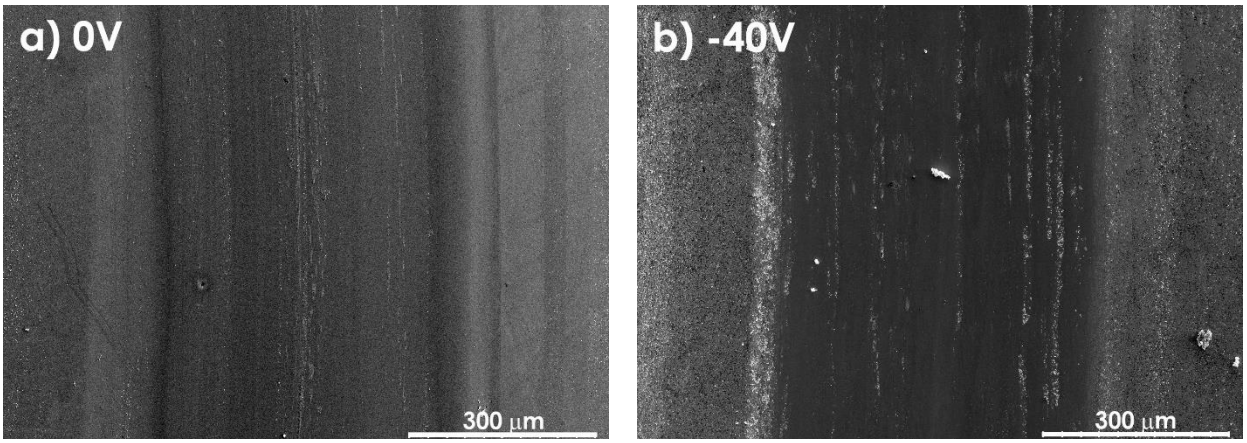

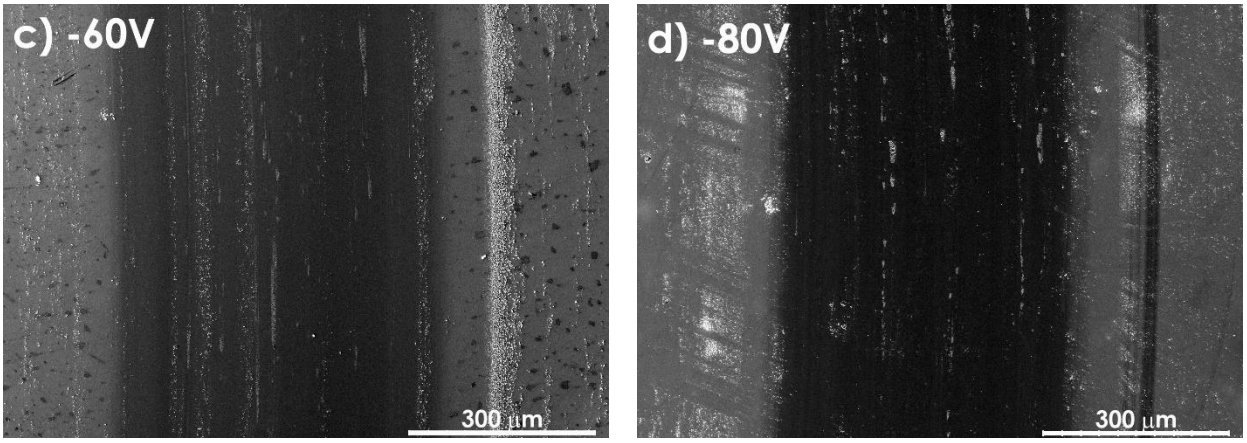

Figure 4.9. SEM micrographs of tracks left from tribology testing for substrate polarisation of: a) 0 V; b) -40 V; c) -60 V; d) -80 V.

The composition of both pin and film post-testing is collected in Table 4.2 and Table 4.3, respectively. The tables have the results measured in untested and clean samples and standard pin that are used as reference, labelled as "FILM" or "PIN" in the respective table.

(V)		**0**		**-40**		**-60**		**-80**	
	PIN	**transf**	**worn**	**transf**	**worn**	**transf**	**worn**	**transf**	**worn**
W	-	4.9	-	5.8	-	9.9	-	6.8	-
C	14.6	8.3	9.4	9.3	9.9	11.3	9.6	12.0	11.6
Ti	-	5.7	-	5.8	-	9.0	-	7.1	-
N	-	2.8	-	2.8	-	4.5	-	1.5	-
Cr	1.2	-	1.2	-	1.6	-	1.5	-	1.0
Fe	81.4	38.8	89.5	40.0	88.5	3.7	88.9	21.6	87.4
O	2.9	39.6	-	36.2	-	61.5	-	51.0	-

Table 4.2 Composition obtained by EDS of wear pins used in WCTiN films testing of "bias series" measured on the contact point. PIN represents the composition reference on clean and unused pin; "trasf" corresponds to composition measured on particles in the contact point; and "worn" to the worn contact point of the pin.

The respective composition of the pin and film were then used to infer the respective transfer from the film to the pin and vice-versa that occurred during the pin-on-disk tests. In the pin is clear the appearance of W, Ti and N from the film, and a decrease of Cr and Fe resulting in a lower signal from the pin. A significant increase of O is also obtained, suggesting some oxidation of the released debris (debris either from the pin or from the film). In the worn areas, the composition is similar when compared to clean and unused pin.

The composition analysed in the film shows similar but inversed behaviour. In this case, in the debris area, the film composition shows a reduction of elements quantity (W, Ti, C and N) together with signals from the pin (Fe) and increased O signal from oxidation. In

the worn areas, the film composition appears closer to the initial unused film without the oxygen signal. In this last case, we can conclude that the film maintains the composition and does not show signs of surface oxidation resulting from the pin-on-disk testing.

(V)		0		-40		-60		-80	
	FILM	**debris**	**worn**	**debris**	**worn**	**debris**	**worn**	**debris**	**worn**
W	15.5	12.5	13.7	10.9	16.5	12.1	15.6	12.4	13.4
C	28.5	16.2	20.7	11.2	20.1	17.5	25.8	20.5	23.0
Ti	11.2	15.7	18.2	11.6	17.8	9.1	13.1	11.7	16.8
N	39.2	24.6	40.8	10.1	40.2	16.4	40.6	32.1	41.9
Fe	1.9	2.5	3.3	7.7	2.3	1.2	2.9	1.5	2.1
O	3.8	28.5	3.3	48.5	3.2	43.7	2.1	21.7	2.9

Table 4.3 Composition obtained by EDS of wear track from WCTiN film "bias series" measured in the wear track. "Film" represents the composition reference on clean and unused WCTiN coating; "debris" corresponds to composition measured on particles in the wear track; and "worn" to the wear track of the coating.

Figure 4.10 represents a graphic visualization of data for specific wear rate on both pin (a) and WCTiN film (b), post tribology testing and measurement with profilometer.

Results on specific wear rate are rather interesting. To start off, sample -40 V outputs a strange behaviour, that despite clearly showing a harder coating than 0 V sample (Figure 4.5), it still measured the highest specific wear rate, both in the pin and in the film, across both series. The films at -60 V and -80 V have the lowest and similar values. Their pin, on the other hand, only the -60 V sample also shows lower specific wear rate.

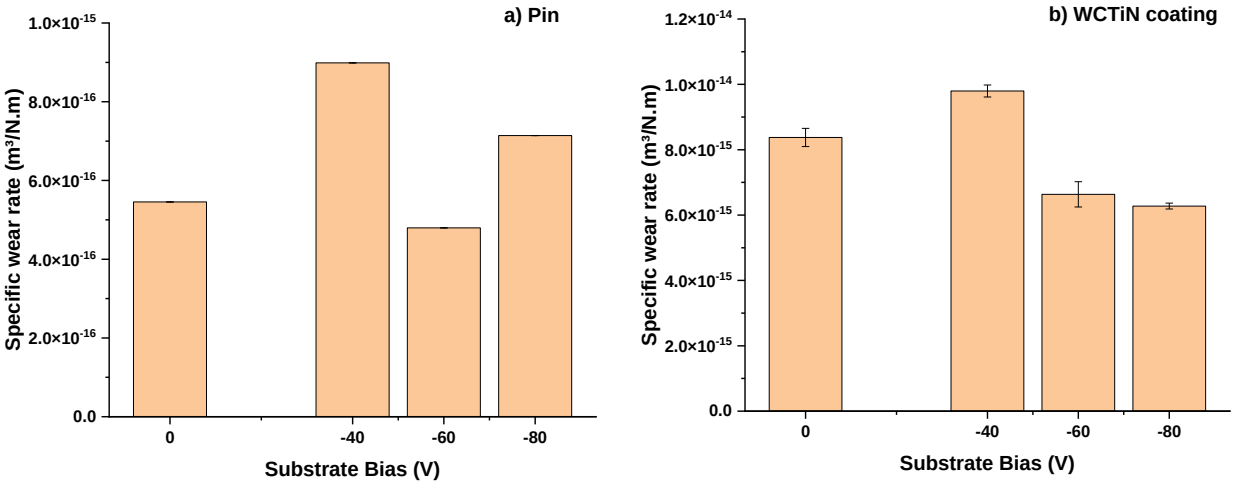

Figure 4.10. Specific wear rate obtained for different substrate polarisation post pin-on-disk testing: a) pin; b) WCTiN coating.

4.2. PP series

4.2.1. Composition

The composition for the thin films of WCTiN with increasing peak power (PP) is presented in Figure 4.11.

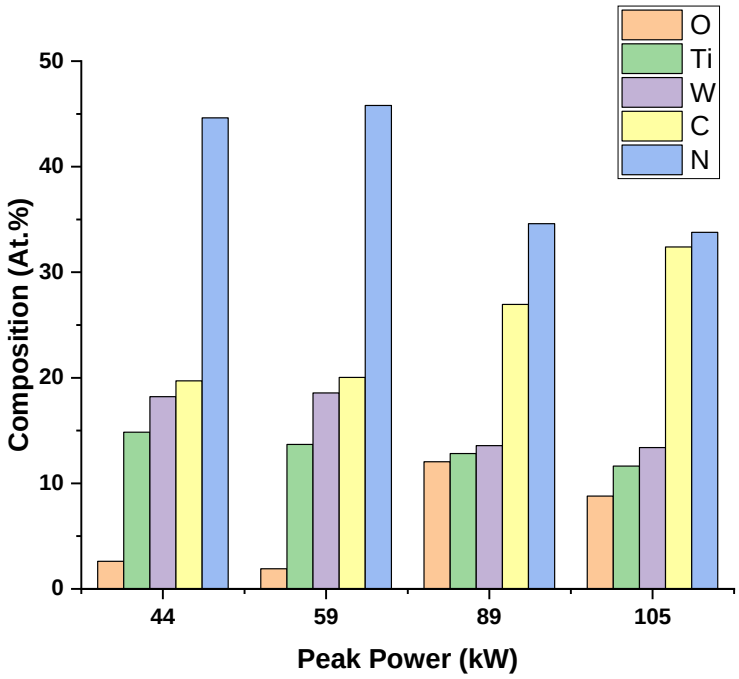

Figure 4.11. Composition of WCTiN with different peak power obtained through EDS.

The composition of these films shows considerable changes. Starting with N, at 44 kW and 59 kW have about the same at. % at 45 %, then decreasing to around 34 % for both 89 kW and 105 kW. Equal behaviour is seen with O, being 2.6 % and 1.9 % respectively for 44 kW and 59 kW and then rising to around 12 % and 9 % for 89 kW and 105 kW, respectively. Ti concentration shows inverse proportionality between its amount and peak power variation, steadily decreasing from 15 % to 12 %. Tungsten behaviour is similar to N and O, having similar values for 44 kW and 59 kW (around 18 %) and then dropping to 14 % for 89 kW and 105 kW. C element also has a correlation of composition with the peak power increase, increasing along with peak power from 20% on both 44 kW and 59 kW, to 32 % on 89 kW and 105 kW.

4.2.2. Structure

The XRD spectra of the WCTiN films prepared with varying peak power are displayed in Figure 4.12.

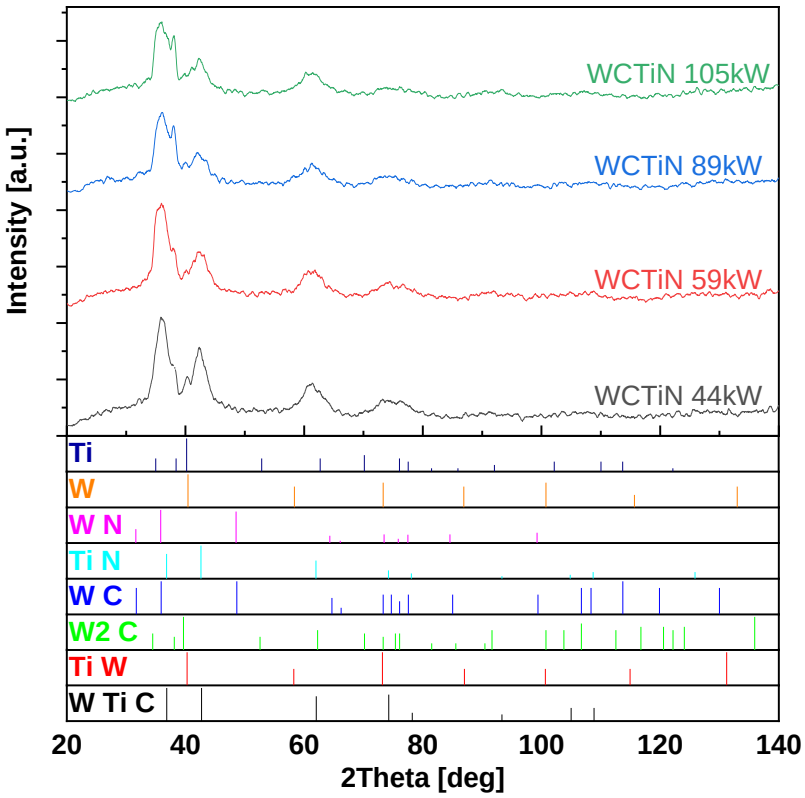

Figure 4.12. XRD spectra of WCTiN films for varying peak power. The reference pattern for Ti, W, WN, TiN, WC, W2C, TiW and WTiC are also displayed in the spectra.

The WCTiN films with increasing peak power have a more substantial influence on film structure. Shifting of the corresponding low intensity WTiC peaks still appear for all the samples, confirming the influence of N on WCTiN formation. In this case, it is also noticed that for increasing peak power less sharp the XRD peaks become. This can be attributed to the increasing bombarding energy during film growth obtained with the PP increase. The results continue to show traces of WC peaks throughout the different specimens, but no complete indexation is obtained, confirming the decarburization of WC during the sputtering process. TiN, TiW and WN display partially indexed peaks which further corroborates WC decarburization.

4.2.3. Microstructure

The microstructure of the WCTiN thin films can be viewed in Figure 4.13 for the cross-section of the samples prepared with different peak power.

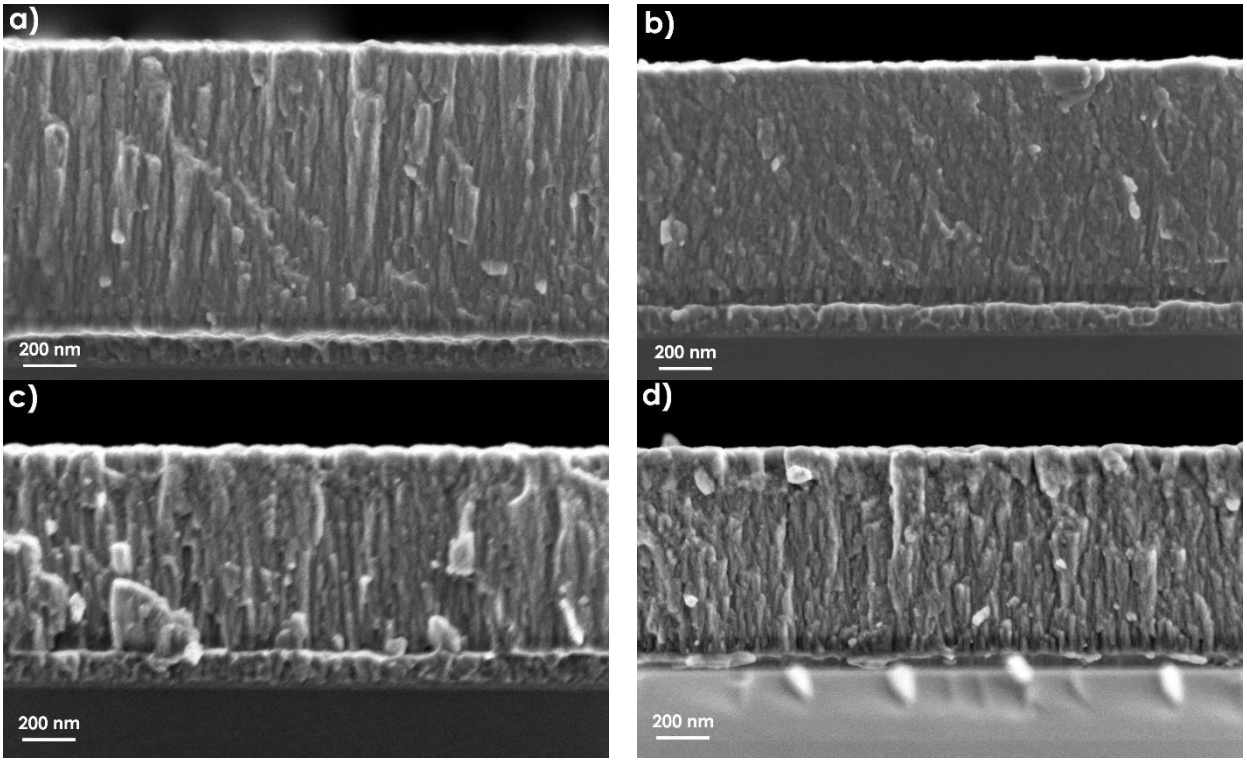

Figure 4.13. SEM cross-section micrographs of WCTiN films prepared with peak power of: a) 44 kW; b) 59 kW; c) 89 kW; d) 105 kW.

The SEM micrographs confirm that changing the peak power on the Ti target has strong effect on the microstructure of the films. The microstructure evolves from completely columnar to denser, where the columns become more difficult to distinguish.

4.2.4. Surface morphology

In Figure 4.14 are presented the surface SEM micrographs of the WCTiN films prepared with increasing peak power.

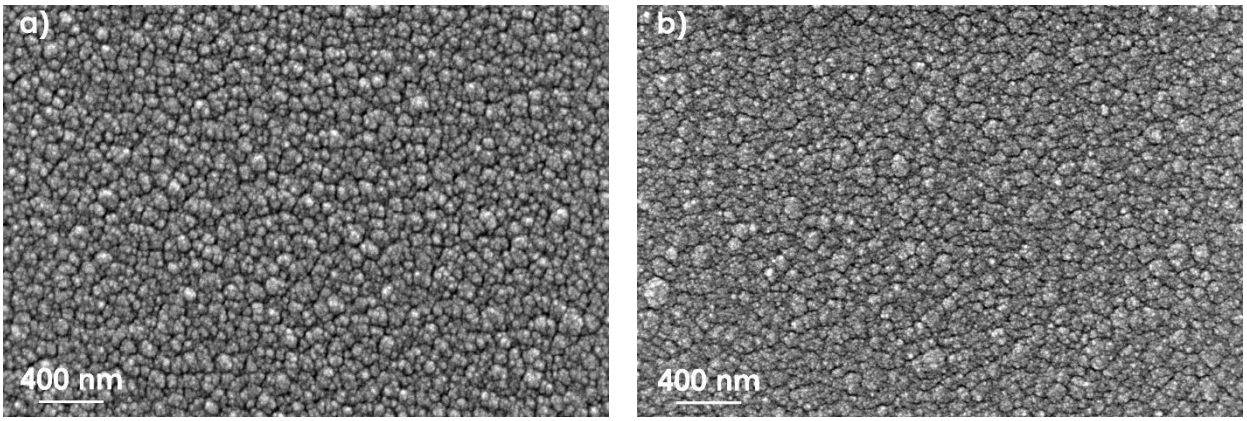

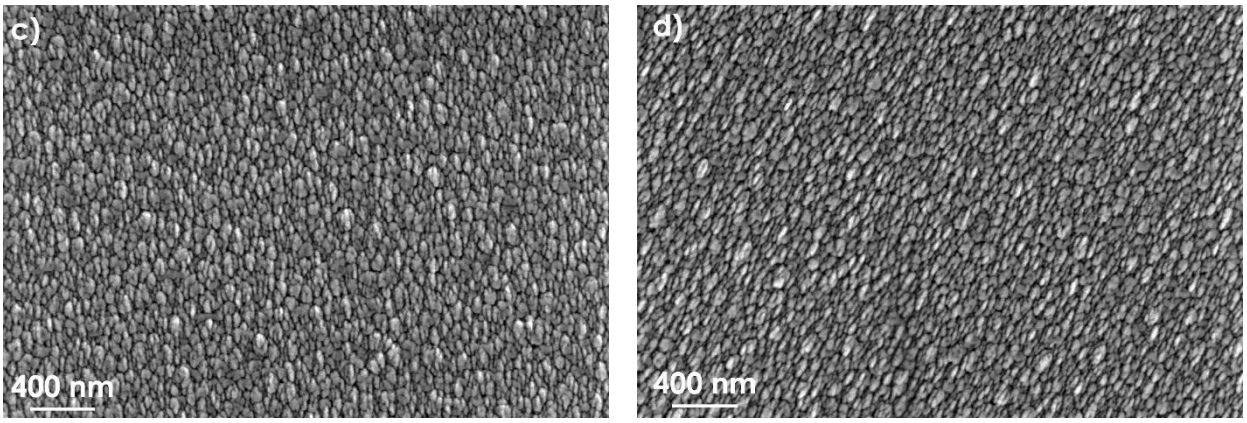

Figure 4.14. SEM photos of surface for different peak power applied on samples at 30.00x magnification: a) 44 kW; b) 59 kW; c) 89 kW; d) 105 kW.

The surface micrographs of WCTiN film prepared with different peak power show a transition from cauliflower-type microstructure (a and b micrographs) to grainy-type (micrographs c and d). The increase in peak power from 89 kW to 105 kW adds directional microstructure to the film, showing elongated grains.

The surface roughness parameters obtained with AFM are presented in Table 4.4.

Peak p. (kW)	**44**	**59**	**89**	**105**
S_q (nm)	6.41	5.73	5.64	3.53
Skew	0.33	0.49	0.50	0.50

Table 4.4 AFM surface roughness measurements for WCTiN PP samples.

The films have decreasing roughness values with an increase in peak power. This change in surface morphology is a complement to the data already seen in Figure 4.14 where the microstructure is also changing with peak power.

4.2.5. Mechanical properties

The evaluation of WCTiN thin film mechanical properties is displayed in Figure 4.15. Variation of peak power on the titanium target does not correspond with obvious changes in both hardness and Young's modulus of the films. All the films recorded around 20 GPa hardness value with a slightly lower value for the 89 kW at 17 GPa, highest for 105 kW at nearly 21 GPa.

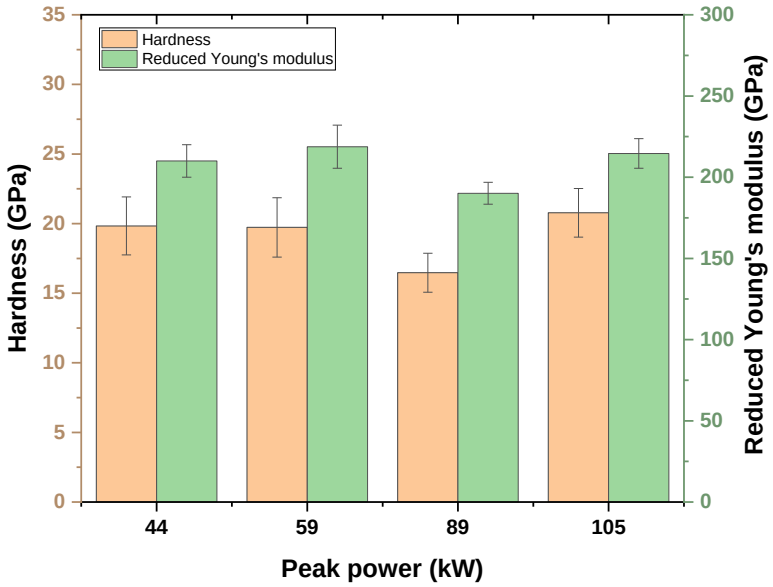

Figure 4.15. Hardness and reduced Young's modulus taken with 5mN load for WCTiN films prepared with different peak power.

The maximum depth achieved during the nano-hardness measurements is detailed in Table 3.3. The results, as in the previous bias series, confirm that during the measurements, we can exclude significant substrate influence from hardness results.

Performed scratch testing on the varying peak power specimens can be seen in Figure 4.16. Note that the WCTiN sample of 59 kW PP is shown in Figure 4.6 b). The testing on PP series and bias series were done on different occasions and resulted in differing optical scales, despite being utilized the same equipment and software.

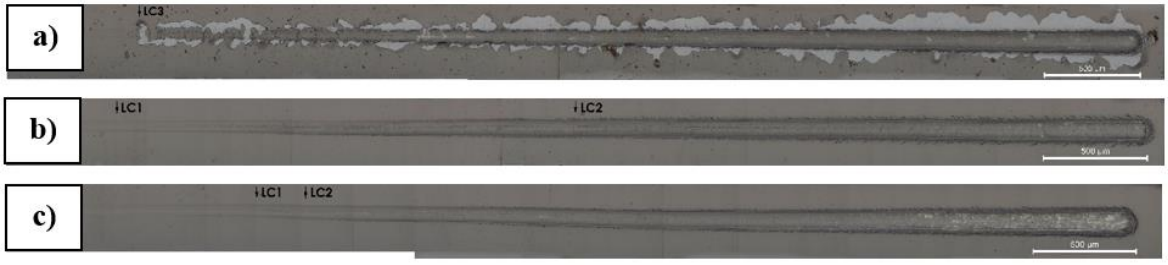

Figure 4.16. Optical images of scratches of WCTiN films with peak power of: a) 44 kW; b) 89 kW; c) 105 kW.

The results show that optimal adhesion is obtained for around 59 kW and 89 kW samples. The 44 kW sample has a critical LC3 type failure at 8.8 N of force. The best performing sample is the sample with 59 kW (Figure 4.6 b) and 89 kW (Figure 4.16 b) peak power with LC2 failure only after 34.8 N and 33.0 N, respectively, although both with an early LC1 type failure at 3.4 N and 11.3 N, respectively. The 105 kW sample shows the latter LC1 at 18.2 N but then cracking occurs quickly with LC2 at 20.6 N.

4.2.6. Tribological properties

The CoF values measured from pin-on-disk test for the WCTiN films prepared with different peak power are presented in Figure 4.17.

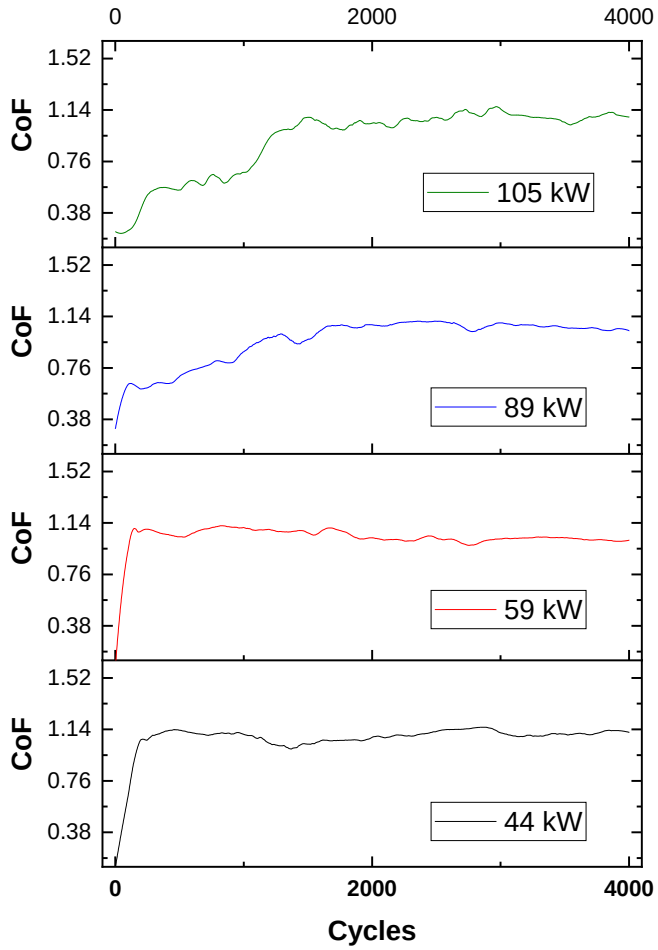

Figure 4.17. CoF results of WCTiN films obtained from pin-on-disk test ran for approximately 200 m with a load of 5 N.

The results, unlike previous values of bias series of Figure 4.7, indicate that there is influence of the peak power on CoF behaviour. The CoF values after reaching the steady state are similar around 1.1 in all samples, but the CoF development until the steady state is different. Noticeably, the lower peak power samples, namely 44 kW and 59 kW samples, show similar behaviour that is also similar to the behaviour of bias series samples (Figure 4.7). Their running-in if fast and sharp until the steady state value. On the other hand, the 89 kW and 105 kW samples have smaller running-in CoF value reached, having then continuous smoother increase of CoF until reaching the steady state value after 2000 cycles.

SEM micrographs of the pin-on-disk pins after the tribology testing are shown in Figure 4.18.

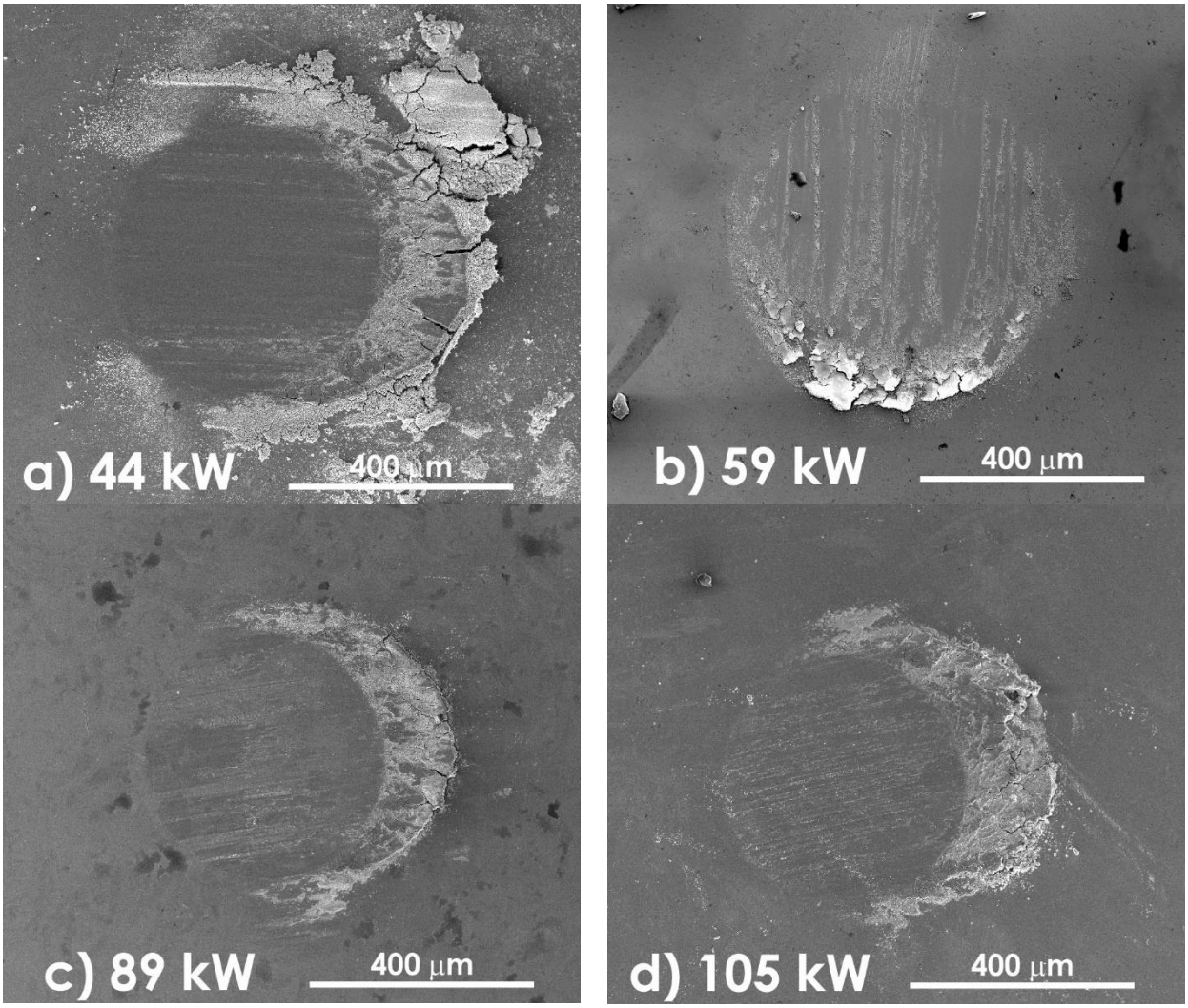

Figure 4.18. SEM micrographs of pin contact point during the tribology testing for peak power of: a) 44 kW; b) 59 kW; c) 89 kW; d) 105 kW.

All but the 59 kW specimen have relatively equal areas of the contact point. The 59 kW sample worn volume is considerably higher as a result of higher wear. This sample also shows more area with film-transferred material (SEM white zones in the contact area).

The SEM micrographs obtained from the wear tracks after pin-on-disk testing of the WCTiN films prepared with increasing PP are shown in Figure 4.19. Unlike biasing effect (Figure 4.9), the wear tracks micrographs registered indicate a corelation between PP and track width. Film prepared with 44 kW and 59 kW are visibly larger than 89 kW and 105 kW. At 44 kW it is also attained the cleanest wear track throughout this study.

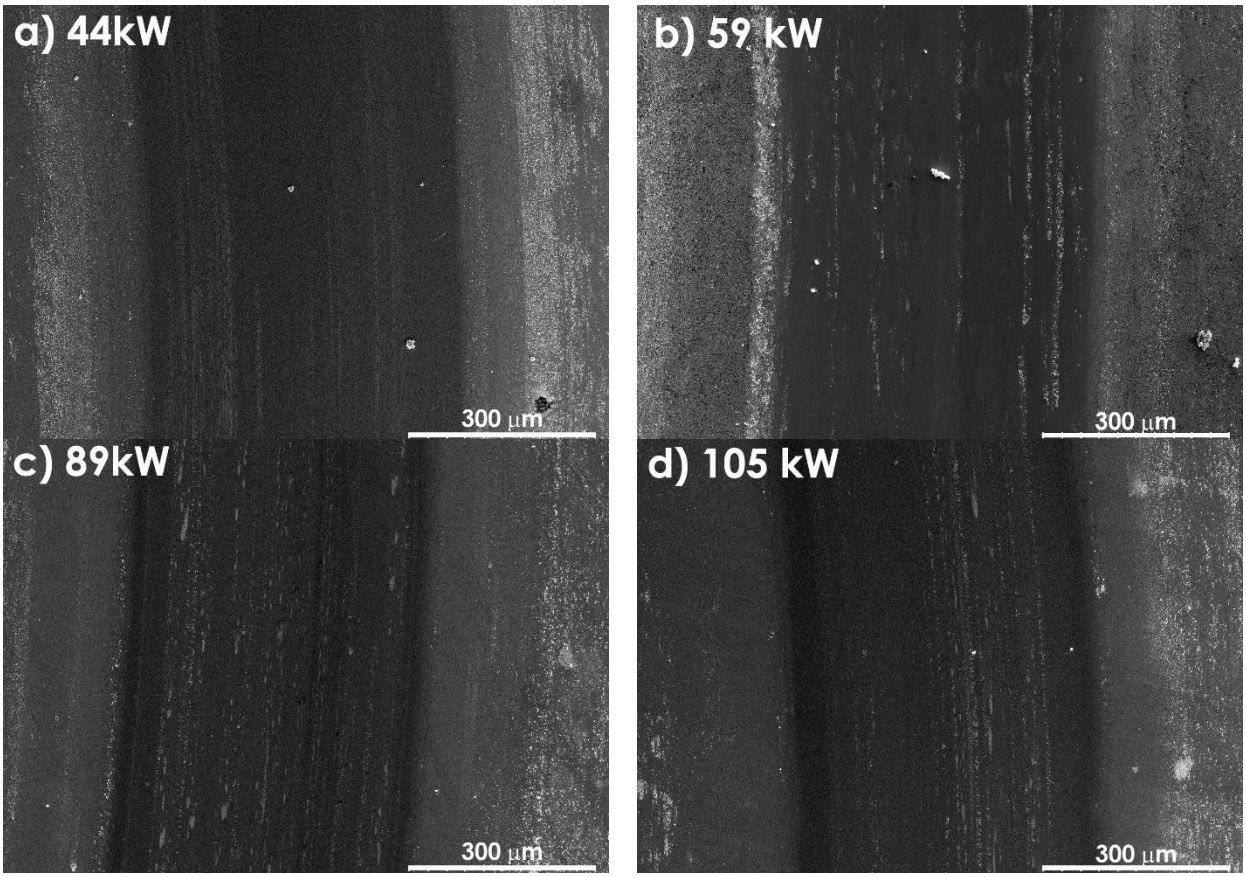

Figure 4.19. SEM micrographs of tracks left from tribology testing for peak power of: a) 44 kW; b) 59 kW; c) 89 kW; d) 105 kW.

In Table 4.5 and Table 4.6 are presented EDS composition results obtained in the films worn pin and wear track, respectively.

(kW)		44		59		89		105	
	PIN	**transf**	**worn**	**transf**	**worn**	**transf**	**worn**	**transf**	**worn**
W	-	10.7	-	5.8	-	8.8	-	10.3	-
C	14.6	11.7	8.9	9.3	9.9	11.3	14.9	10.8	12.8
Ti	-	7.8	-	5.8	-	10.7	-	11.3	-
N	-	3.1	-	2.8	-	2.4	-	2.5	-
Cr	1.2	-	1.4	-	1.6	-	0.1	-	1.4
Fe	81.4	13.9	82.7	40.0	88.5	4.4	83.2	4.2	85.5
O	2.9	52.5	-	36.2	-	62.4	-	61.0	-

Table 4.5. Composition obtained by EDS performed in the contact point of the pins from series PP. PIN represents the composition reference on clean and unused pin; “transf” corresponds to composition measured on particle in the contact point; and “worn” to the worn contact point of the pin.

The composition results show similar behaviour like in bias series. In the pin there is signs of film transfer (W, Ti and N) and increased O resulting from oxidation, while in the film opposite situation is verified, with increase of Fe from pin transfer and increase of O from oxidation process.

(kW)		44		59		89		105	
	FILM	**debris**	**worn**	**debris**	**worn**	**debris**	**worn**	**Debris**	**worn**
W	15.5	17.3	16.5	10.9	16.5	8.1	11.6	10.8	11.2
C	28.5	23.8	22.9	11.2	20.1	11.9	16.7	18.6	18.7
Ti	11.2	15.6	17.7	11.6	17.8	22.5	25.4	26.0	25.5
N	39.2	38.4	38.1	10.1	40.2	16.3	36.3	31.0	34.8
Fe	1.9	2.9	3.1	7.7	2.3	8.0	7.5	7.7	7.8
O	3.8	2.1	1.7	48.5	3.2	33.2	2.5	5.7	2.1

Table 4.6 Composition obtained by EDS performed in the worn tracks from series PP. PIN represents the composition reference on clean and unused pin; "transf" corresponds to composition measured on particle in the contact point; and "worn" to the worn contact point of the pin.

The wear rate results for the WCTiN films prepared with different peak power and the respective pin are presented in Figure 4.20 a) and b), respectively.

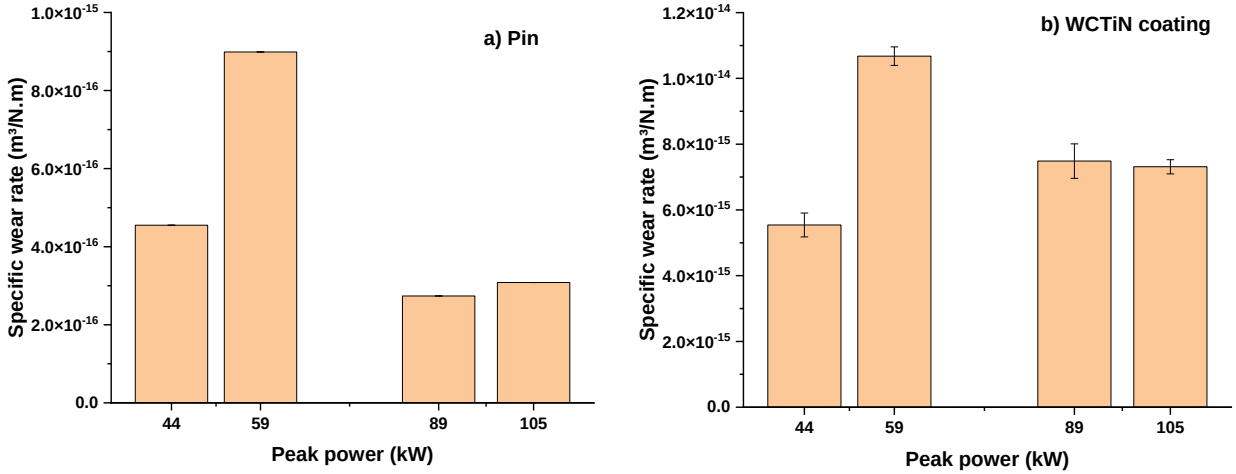

Figure 4.20. Specific wear rate of WCTiN films of different peak power after pin-on-disk testing of a) pin; b) WCTiN coating. No error on b) due to too small of a scale.

Specific wear rate highest value is obtained for the 59 kW peak power sample, both on pin (around 9.0x10-16 m3/N.m) and coating (1.1x10-14 m3/N.m). This sample is the equivalent of -40 V from bias series, confirming that it is the highest value of both series. The lowest specific wear rate was obtained for 44 kW film although the pin corresponding specific wear is not the lowest. The CoF initial behaviour can have influence in the system wear. The samples 89 kW and 105 kW have similar values for both pin and film wear. This wear behaviour can be correlated with the different surface morphology noticed, Figure 4.14 b and c.

5. DISCUSSION

Although the work here presented consists of an early study on the mechanical and tribological properties of WCTiN films, this transition metal tungsten carbonitride merits follow-up research based, if not by its element constitution and growing relevance in the current industry, then by its cooperative nature with this recent development co-sputtering method, combining the high deposition rates provided by DCMS and the denser film growth capabilities praised within DOMS technology. The analysis consisted in increasing substrate polarisation and peak power, and, in theory, both should increase the density of the thin films and modify properties consequently.

5.1. BIAS series

In the substrate polarisation series, the seemingly best performing film was the one prepared with -60V of substrate polarisation. This film has the highest hardness at 29 GPa (Figure 4.5), surpassing other W-C-Ti based coatings, which are typically around 15 to17 GPa [40]. This sample also has good adhesion and a low specific wear rate, together with high CoF.

The structure and composition do not show significant changes among these thin films, having small relation with substrate polarisation variation. On mechanical and tribological properties, the influence is evident. Less negative substrate polarisation has the lowest hardness and Young's modulus. The worse performing sample is the -40 V, with lower adhesion (earlier failure seen in Figure 4.6) and high specific wear rate (the highest between both series, Figure 4.10 and Figure 4.20), even if it is 33 % harder than the 0 V sample. The 0 V sample claims the lowest harness compared to all others. The -80 V sample has the most unstable results. The adhesion is the worst, with complete early delamination, hardness is also strongly reduced, but CoF maintains similar values and also has the lowest specific wear rate of substrate polarisation series.

Overall, the most promising sample is the -60 V, despite not having the lowest specific wear rate on film, it is the most stable with consistent results, plus it only has a slightly higher wear measurement by 0.17x10-15 m3/N.m, than the -80 V in Figure 4.10 b, an amount that can be dismissed based on the inconsistency in reliable results across this study, explained in chapter 3.9.

5.2. PP series

Unlike the BIAS series, changing the peak power has an effect on the microstructure of the WCTiN films. The cross-section and surface morphology SEM micrographs (Figure 4.13 and Figure 4.14) show denser film and influenced surface morphology with increase of peak power, resulting in the decrease of the surface roughness. Mechanically speaking, hardness (Figure 4.15) did not seem particularly linked to PP as all samples rounded the same 20 GPa, exempting the 89 kW sample that suffered a 3 GPa loss compared to the average. Adhesion (Figure 4.16) clearly benefits from the increased peak power up to 89 kW. The 44 kW sample had an immediate critical failure, and the 105 kW has LC2 type failure considerably sooner than 59 kW and 89 kW. Among these two, 59 kW performed slightly better and, together with hardness, seems to be the optimal point for mechanical properties. However, tribology testing confirms that the 89 kW exceeds 59 kW meaningfully. CoF results (Figure 4.17) have two distinct behaviours, one on 44 kW and 59 kW pair with low and long running-in. The 89 kW and 105 kW pair have fast and short running-in period, like BIAS series. Their specific wear rate (Figure 4.20) shows better performance for higher PP samples.

Recommendation based on all results would be to further study on 89 kW or slightly below, as the 59 kW marginally outperformed on mechanical properties.

6. CONCLUSIONS

Thin WCTiN films were successfully deposited via co-sputtering of tungsten carbide target with DCMS and titanium with HiPIMS, in a reactive nitrogen environment. The application of substrate polarisation and variation of the HiPIMS peak power proved to influence the final WCTiN film properties, being possible to establish an important conclusion. This could provide to be useful in industries that require high quality coatings with desirable properties that are sustained in aggressive environments, where TiCN/TiN-based cermets have proven desirable [1 - 4].

Composition-wise, peak power influence has a great effect on all constituent elements with the exception of Ti, while substrate polarisation manipulation had little effect. The same phenomenon occurred on structure and microstructure, again PP had a reasonable impact on the thin film with a noticeable increase in density, while substrate biasing did not. Surface roughness was only directly impacted by peak power together with added directionality and changing from cauliflower-type (seen throughout bias series) to elongated granules.

Regarding hardness, the highest reached value was for -60 V substrate polarisation with 29 GPa, while on PP, all averaged 19 GPa. To summarize, only substrate biasing affected these properties up to an optimal point before its steep decline, directly correlated to adhesion failure.

For coefficient of friction all samples settled around 1.1 with low PP samples (44 kW and 59 kW) deviating from the similar conduct observed on all others, with these two having a longer running-in. Despite the good results of 44 kW sample during testing, including lowest specific wear rate of all tested films, critical failure occurred very early on scratch test. The 105 kW sample suffers from the same fate as the 44 kW, good results accompanied by poor adhesion, so it can be recommended that further investigation proceeds with the development of better performing interlayer establishing the use of the film in harsher environments [13].

Analysis from the study performed on this newly WCTiN thin film indicate that there is potential in further research, recommended as starting point with the use of this co-sputtering process composed on DCMS and DOMS technology with -60 V substrate polarisation and somewhere between 59 kW and 89 kW for peak power on HiPIMS source.

7. FUTURE WORK

Regarding the development of this new WCTiN thin film, it can be recommended that further investigation is made on peak power and substrate biasing using as starting points the best performing referred in this work.

Another recommendation is on further work to be done with the interlayer. Promising specific wear rate results were obtained on unrecommended samples. For example, the lack of adhesion is surely responsible for the -80 V sample low hardness, however, this sample still has remarkable low wear. Another good example was the fact that the 105 kW sample reached the highest hardness with equally low critical adhesion failure. In both cases improved adhesion can represent enough improvement to turn those samples into good performing systems.

As the literature used for this study suggests, this type of material could be very beneficial to the industry of cutting tools and wear resistance coatings, further analysis into that field should be explored in real testing conditions.

8. REFERENCES

1 – Weigert, E. C., Humbert, M. P., Mellinger, Z. J., Ren, Q., Beebe Jr, T. P., Bao, L., & Chen, J. G. (2008). Physical vapor deposition synthesis of tungsten monocarbide (WC) thin films on different carbon substrates. *Journal of Vacuum Science & Technology A: Vacuum, Surfaces, and Films*, 26(1), 23-28.

2 – Peng, Y., Miao, H., & Peng, Z. (2013). Development of TiCN-based cermets: Mechanical properties and wear mechanism. *International Journal of Refractory Metals and Hard Materials*, 39, 78-89.

3 – Akinribide, O. J., Obadele, B. A., Akinwamide, S. O., Bilal, H., Ajibola, O. O., Ayeleru, O. O., ... & Olubambi, P. A. (2019). Sintering of binderless TiN and TiCN-based cermet for toughness applications: processing techniques and mechanical properties: a review. *Ceramics International*, 45(17), 21077-21090.

4 – Pattnaik, S. K., Bhoi, N. K., Padhi, S., & Sarangi, S. K. (2018). Dry machining of aluminum for proper selection of cutting tool: tool performance and tool wear. *The International Journal of Advanced Manufacturing Technology*, 98(1), 55-65.

5 – Tsai, M. H. (2013). Physical properties of high entropy alloys. *Entropy*, 15(12), 5338-5345.

6 – Basu, I., & De Hosson, J. T. M. (2020). Strengthening mechanisms in high entropy alloys: fundamental issues. *Scripta Materialia*, 187, 148-156.

7 – Ferreira, F., Cavaleiro, A., & Oliveira, J. (2020). Effect of the Substrate Biasing on the Structure and Properties of Tantalum Coatings Deposited Using HiPIMS in Deep Oscillations Magnetron Sputtering Mode. *Metals*, 10(12), 1618.

8 – Ferreira, F., Cavaleiro, A., & Oliveira, J. (2021). Effect of Peak Power in Deep Oscillation Magnetron Sputtering on Film Properties. *Journal of Materials Engineering and Performance*, 30(6), 3912-3924.

9 – Kelly, P. J., & Arnell, R. D. (2000). Magnetron sputtering: a review of recent developments and applications. *Vacuum*, 56(3), 159-172.

10 – Öztürk, A., Ezirmik, K. V., Kazmanlı, K., Ürgen, M., Eryılmaz, O. L., & Erdemir, A. (2008). Comparative tribological behaviors of TiN, CrN and MoNCu nanocomposite coatings. *Tribology International*, 41(1), 49-59.

11 – Voevodin, A. A., O'neill, J. P., & Zabinski, J. S. (1999). WC/DLC/WS2 nanocomposite coatings for aerospace tribology. Tribology Letters, 6(2), 75-78.

12 – Pirso, J., Viljus, M., & Letunovitš, S. (2006). Friction and dry sliding wear behaviour of cermets. *Wear*, 260(7-8), 815-824.

13 – Cicek, H. (2018). Wear behaviors of TiN/TiCN/DLC composite coatings in different environments. *Ceramics International*, 44(5), 4853-4858.

14 – Je, J. H., Gyarmati, E., & Naoumidis, A. (1986). Scratch adhesion test of reactively sputtered TiN coatings on a soft substrate. *Thin Solid Films*, 136(1), 57-67.

15 – Zuñega, J. C. P., Gee, M. G., Wood, R. J. K., & Walker, J. (2012). Scratch testing of WC/Co hardmetals. *Tribology international*, 54, 77-86.

16 – Gee, M. G., Gant, A., & Roebuck, B. (2007). Wear mechanisms in abrasion and erosion of WC/Co and related hardmetals. *Wear*, 263(1-6), 137-148.

17 – Cavaleiro, A., & Vieira, M. (1995). *Engenharia de superfícies e degradação e protecção de superfícies*. Departamento de Engenharia de Mecânica.

18 – Baptista, A., Silva, F., Porteiro, J., Míguez, J., & Pinto, G. (2018). Sputtering physical vapour deposition (PVD) coatings: A critical review on process improvement and market trend demands. *Coatings*, 8(11), 402.

19 – Ferreira, F.E.D.S., 2013. *Pulverização catódica magnetrão com impulsos de alta potência (HiPIMS) em modo DOMS* (Master dissertation, Universidade de Coimbra).

20 – Swann, S. (1988). Magnetron sputtering. *Physics in technology*, 19(2), 67.

21 – Bräuer, G., Szyszka, B., Vergöhl, M., & Bandorf, R. (2010). Magnetron sputtering–Milestones of 30 years. *Vacuum*, 84(12), 1354-1359.

22 – Safi, I. (2000). Recent aspects concerning DC reactive magnetron sputtering of thin films: a review. *Surface and Coatings Technology*, 127(2-3), 203-218.

23 – Depla, D., & De Gryse, R. (2004). Target poisoning during reactive magnetron sputtering: Part I: the influence of ion implantation. *Surface and Coatings Technology*, 183(2-3), 184-189.

24 – Depla, D., & De Gryse, R. (2004). Target poisoning during reactive magnetron sputtering: Part II: the influence of chemisorption and gettering. *Surface and Coatings Technology*, 183(2-3), 190-195.

25 – Ferreira, F. E. D. S. (2018). *Process-properties relations in deep oscillation magnetron sputtering* (Doctoral dissertation, 00500: Universidade de Coimbra).

26 – Anders, A. (2014). A review comparing cathodic arcs and high power impulse magnetron sputtering (HiPIMS). *Surface and Coatings Technology*, 257, 308-325.

27 – Lin, J., Sproul, W. D., Moore, J. J., Wu, Z., Lee, S., Chistyakov, R., & Abraham, B. (2011). Recent advances in modulated pulsed power magnetron sputtering for surface engineering. *Jom*, 63(6), 48-58.

28 – Ferreira, F., Serra, R., Oliveira, J. C., & Cavaleiro, A. (2014). Effect of peak target power on the properties of Cr thin films sputtered by HiPIMS in deep oscillation magnetron sputtering (DOMS) mode. *Surface and Coatings Technology*, 258, 249-256.

29 – Mukhopadhyay, A., & Basu, B. (2011). Recent developments on WC-based bulk composites. *Journal of Materials Science*, 46(3), 571-589.

30 – Heydari, L., Lietor, P. F., Corpas-Iglesias, F. A., & Laguna, O. H. (2021). Ti (C, N) and WC-Based Cermets: A Review of Synthesis, Properties and Applications in Additive Manufacturing. *Materials*, 14(22), 6786.

31 – Koželj, P., Vrtnik, S., Jelen, A., Jazbec, S., Jagličić, Z., Maiti, S., ... & Dolinšek, J. (2014). Discovery of a superconducting high-entropy alloy. *Physical review letters*, 113(10), 107001.

32 – Sharma, P., Dwivedi, V. K., & Dwivedi, S. P. (2021). Development of high entropy alloys: A review. *Materials Today: Proceedings*, 43, 502-509.

33 – Jien-Wei, Y. E. H. (2006). Recent progress in high entropy alloys. *Ann. Chim. Sci. Mat*, 31(6), 633-648.

34 – Zhang, Y., Zuo, T. T., Tang, Z., Gao, M. C., Dahmen, K. A., Liaw, P. K., & Lu, Z. P. (2014). Microstructures and properties of high-entropy alloys. *Progress in materials science*, 61, 1-93.

35 – Stachowiak, G. W., & Batchelor, A. W. (2013). *Engineering tribology*. Butterworth-heinemann.

36 – Meng, Y., Xu, J., Jin, Z., Prakash, B., & Hu, Y. (2020). A review of recent advances in tribology. *Friction*, 8(2), 221-300.

37 – Gohar, R., & Rahnejat, H. (2018). *Fundamentals of tribology*. World Scientific.

38 – Blau, P. J. (2001). The significance and use of the friction coefficient. *Tribology International*, 34(9), 585-591.

39 – Hovsepian, P. E., Sugumaran, A. A., Purandare, Y., Loch, D. A., & Ehiasarian, A. P. (2014). Effect of the degree of high power impulse magnetron sputtering utilisation on the structure and properties of TiN films. *Thin solid films*, 562, 132-139.

40 – Koutzaki, S. H., Krzanowski, J. E., & Nainaparampil, J. J. (2002). Phase formation and microstructure in sputter-deposited Ti-Mo-C and Ti-WC thin films. *Metallurgical and Materials Transactions A*, 33(6), 1579-1588.